ASM | Microbiology Spectrum

| Open Peer Review | Mycology | Research Article

Morphotype-specific susceptibility to *Neosartorya* (*Aspergillus*) *fischeri* antifungal protein 2 is associated with an anabolic transcriptional signature in *Candida*

Richárd Merber,[1,2] Krisztián Laczi,[1,3] Gábor Bende,[1,2,4] Erika Kazinczi,[1] Attila Farkas,[3] Gergely Maróti,[3] Rita Sinka,[5] László Galgóczy[1]

AUTHOR AFFILIATIONS See affiliation list on p. 20.

ABSTRACT The emergence of drug-resistant *Candida* species has created a demand for global antifungal strategies that extend beyond classical growth inhibition to target unknown vulnerabilities of fungal pathogens. In this study, we demonstrated that the *Neosartorya* (*Aspergillus*) *fischeri* antifungal protein NFAP2 selectively targets early morphogenetic states of *Candida albicans* and *Candidozyma auris*, revealing a transient window of susceptibility during filament and pseudohypha formation. Integrated transcriptomic and *in vivo* analyses indicate that these developmental states may represent context-dependent entry points for NFAP2 activity. In *C. albicans*, transcriptomic and network analyses indicate the presence of an anabolic, translation-associated gene expression signature, accompanied by suppression of stress-protective pathways, which is associated with increased susceptibility of emerging hyphae to NFAP2 but does not establish a direct causal mechanism. In *C. auris*, increased susceptibility of pseudohyphal cells occurred without overt transcriptional remodeling, consistent with the characteristically muted gene expression responses of this species, suggesting that NFAP2 sensitivity is governed primarily by biophysical and post-transcriptional mechanisms rather than transcriptional reprogramming. Importantly, morphotype-specific vulnerabilities observed *in vitro* were reflected in distinct *in vivo* outcomes in *Galleria mellonella*, as NFAP2 was well tolerated and provided a moderate, transient survival benefit in pseudohyphal *C. auris* infections, but not in filamentous *C. albicans*, where a worsened outcome was observed, consistent with species- and morphotype-dependent activity. Taken together, these results suggest that early morphogenetic states of *Candida* are stress-sensitive phenotypes associated with increased susceptibility to NFAP2. This work provides a proof-of-concept framework for future investigation of morphotype-associated antifungal vulnerability to peptide-based antifungal strategies.

IMPORTANCE Drug-resistant *Candida* species represent an escalating global health threat; however, most antifungal strategies continue to target fungal growth rather than intrinsic biological vulnerabilities. In this study, we identified early morphogenetic transitions as a shared window of increased susceptibility in both *Candida albicans* and the highly drug-resistant pathogen *Candidozyma* (formerly *Candida*) *auris*. By integrating transcriptomic profiling with *in vivo* infection models, we found that NFAP2 exhibits antifungal activity that is influenced by these transient developmental states in a context-dependent manner while remaining well tolerated by the host. We further demonstrated that morphotype-specific stress responses are associated with the divergent sensitivities of *C. albicans* and *C. auris* to NFAP2. These results support the concept that fungal morphogenesis may represent a therapeutically actionable process and provide a framework for designing antifungal strategies that target developmental states rather than growth. This strategy may open new opportunities for improving

Editor Gustavo H. Goldman, Universidade de Sao Paulo Campus de Ribeirao Preto, Sao Paulo, Brazil

Peer Reviewer Octávio Luiz Franco, Universidade Catolica de Brasilia Centro de Analises, Brasilia, Brazil

Address correspondence to László Galgóczy, galgoczi@bio.u-szeged.hu.

The authors declare no conflict of interest.

See the funding table on p. 21.

Received 2 February 2026
Accepted 4 June 2026
Published 6 July 2026

protein- and peptide-based therapies, as well as combination therapies against difficult-to-treat fungal pathogens.

KEYWORDS antifungal protein, *Candida* morphogenesis, morphotype-specific susceptibility, transcriptomic profiling, *in vivo* infection model

The World Health Organization has classified *Candida albicans* and *Candidozyma* (formerly *Candida*) *auris* as critical-priority pathogens in the Fungal Priority Pathogens List because of their potential to cause severe infections and resistance to antifungal treatment (1). Global surveillance data indicate the continuous spread of *C. auris*, with over 4,500 new cases reported in the United States in 2023, which highlights the need for effective preventive measures (2, 3). Although *C. auris* has emerged as a serious multidrug-resistant pathogen, *C. albicans* remains the predominant cause of invasive candidiasis worldwide, particularly in immunocompromised hosts (4, 5). The prevalence of antifungal resistance in these species has made candidiasis an escalating global health concern (6).

Clinical isolates of *C. albicans* and *C. auris* exhibit remarkable morphogenetic flexibility. This enables the transition between yeast and filamentous forms, which is a key virulence attribute (7–9). This morphological switching promotes adaptation to distinct host environments and facilitates tissue invasion, evasion of immune responses, and biofilm formation, all of which enhance the pathogenicity and resistance to antifungal agents (10–12). Filamentation is a widespread and strain-dependent feature among *C. albicans* isolates and a general trait in *C. auris*, which reinforces its role as a virulence determinant (8, 9).

Candida biofilms represent a formidable therapeutic challenge because of their multicellular architecture and enhanced drug resistance. Biofilm-associated cells exhibit increased resistance to antifungal agents, largely attributed to the secreted extracellular matrix, which limits drug penetration, and to biofilm-specific gene expression reprogramming that promotes stress adaptation and resistance (10–13). Consequently, *Candida* biofilms persist on medical devices and tissues, which results in recurrent and chronic infections (14, 15). Although some new antifungal agents, including rezafungin, have become available (16), the development of effective anti-biofilm therapies is limited. Innovative strategies are under development, such as combination therapies, nanotechnology-based delivery systems, and surface modifications to prevent biofilm formation (13).

Antifungal peptides and proteins (AFPs) have recently gained considerable attention as promising agents against *Candida* biofilms. These small, cationic molecules act through multiple mechanisms. They can disrupt fungal membranes, inhibit adhesion and early biofilm development, generate reactive oxygen species, and downregulate genes involved in filamentation and biofilm maintenance (17). AFPs are usually highly selective for fungal cells. They exhibit low cytotoxicity toward mammalian cells, and their multi-targeted mechanisms significantly reduce the emergence of resistance. Nevertheless, large-scale production, *in vivo* stability, and limited pharmacokinetic characterization remain important obstacles to clinical translation (17–19). Importantly, the multifaceted modes of action of AFPs suggest that fungal growth inhibition and intrinsic biological vulnerability can be viewed as interconnected manifestations of underlying physiological states that may be selectively exploited by antifungal agents (20).

Of the AFPs, *Neosartorya* (currently *Aspergillus*) *fischeri* antifungal protein 2 (NFAP2) is a promising candidate. NFAP2 is a small (Mw: 5.6 kDa), cysteine-rich, disulfide-stabilized antifungal protein characterized by a compact, highly stable structure and a strong positive net charge, features that are typical of fungal AFPs with selective membrane and intracellular activity against fungi (21). This protein exhibits selective anti-*Candida* activity, including inhibition of *Candida* filamentation and disruption of biofilms *in vitro* and *in vivo* (22, 23). Previous studies indicate that NFAP2 exhibits a dual mode of action, involving both membrane-associated effects at higher concentrations and

intracellular targeting at sub-inhibitory levels, although the precise molecular mechanisms remain incompletely defined (24). NFAP2 exhibits synergy with conventional antifungals and shows minimal potential to induce resistance in *C. albicans* (25). These physicochemical and functional properties make NFAP2 a suitable model system for investigating morphotype-specific antifungal susceptibility of *Candida*, as its activity is likely influenced by dynamic changes in cell envelope structure, metabolic state, and cellular uptake processes during fungal morphogenesis.

These considerations raise the possibility that transient physiological states associated with early morphogenesis may influence antifungal susceptibility in a context-dependent manner. To advance understanding of NFAP2 activity in clinically relevant settings, it is important to characterize its effects on filamentous *Candida* forms. In this study, we examined the transcriptomic responses of *C. albicans* and *C. auris* filamentous cells exposed to NFAP2. To achieve this, we established a protocol enabling the isolation of early-stage filamentous cells that are not obtainable with conventional biofilm models. Rather than directly testing a single mechanistic pathway, our approach aimed to identify morphotype-associated physiological states that correlate with NFAP2 susceptibility. Our results show that NFAP2 exposure is associated with morphological alterations and transcriptional changes in virulence- and oxidative stress-related pathways, providing the physiological contexts underlying its antifungal activity

RESULTS

Generation of early-stage filamentous *C. albicans* and pseudohyphal *C. auris* cells in aerated liquid culture

To obtain early-stage filamentous *Candida* cells, liquid, aerated culture conditions were established for *C. albicans* CBS 5982 and *C. auris* NCPF 8971. When *C. albicans* was incubated at 37°C for 16 h in AIM V medium at 180 rpm, a heterogeneous population emerged, containing elongated hyphal and planktonic yeast cells. Therefore, additional filtration and washing steps were required to remove the residual planktonic fraction and enrich uniformly filamentous cells (Fig. S1). In contrast, *C. auris* cultures incubated under the same conditions in filamentation-inducing medium (FIM) produced a morphologically homogeneous population, with approximately 90% of the cells exhibiting an elongated pseudohyphal morphology (Fig. S1). No further washing or filtration steps were required for *C. auris*, as the liquid shaking conditions were sufficient to promote synchronous pseudohyphal development. This method facilitated standardized antifungal susceptibility assays on filamentous *Candida* forms, as subsequently demonstrated for determining the minimum inhibitory concentration (MIC) values of NFAP2 against these distinct cell types.

The morphological stability of early-stage filamentous *C. albicans* and pseudohyphal *C. auris* cells was evaluated in low-cation medium (LCM) at 37°C. The freshly prepared *C. albicans* cultures exhibited elongated hyphal morphology with continuous filamentous growth, whereas *C. auris* cells exhibited uniform pseudohyphal forms characterized by visible septal constrictions. For both species, the filamentous and pseudohyphal morphologies remained stable for approximately 2 h, with no detectable reversion to the yeast form. Following this period, *C. albicans* hyphae gradually became fragmented and shortened, showing mixed morphotypes by 5 h (Fig. S2). Similarly, *C. auris* pseudohyphae exhibited reduced elongation and partial reversion after 5 h (Fig. S2). These results indicate that early-stage filamentous *C. albicans* and pseudohyphal *C. auris* maintain their morphological stability for approximately 2 h under LCM conditions at 37°C, which provides a defined experimental window to examine the initial antifungal activity and uptake dynamics of NFAP2.

Filamentous *C. albicans* and pseudohyphal *C. auris* cells show increased susceptibility to NFAP2 compared with planktonic forms

Early-stage filamentous *Candida* cells generated in shaken liquid cultures exhibited markedly higher susceptibility to NFAP2 following a short exposure time (2 h) than their planktonic counterparts. For *C. albicans* CBS 5982, the apparent MIC value for planktonic yeast cells was >3,200 µg mL^{-1}, which did not inhibit growth, whereas the early-stage filamentous cells exhibited an apparent MIC of 6.25 µg mL^{-1}, indicating a marked difference in susceptibility (Fig. 1). A similar trend was observed for *C. auris* NCPF 8971, in which the planktonic form had an apparent MIC >3,200 µg mL^{-1}, whereas the pseudohyphal cells exhibited a markedly lower apparent MIC of 50 µg mL^{-1} (Fig. 1). The observed MIC values are summarized in Table S1. These NFAP2 concentrations completely inhibited colony formation, indicating a strong loss of viability following short-term exposure. This assay reflects post-exposure viability following short-term NFAP2 exposure. Accordingly, filamentous morphotypes of *C. albicans* and *C. auris* are substantially more susceptible to NFAP2 during short-term exposure than their planktonic counterparts, which highlights the morphotype-dependent antifungal activity of this protein.

NFAP2 induces severe ultrastructural alterations in early-stage filamentous *C. albicans* and pseudohyphal *C. auris* cells

Scanning electron microscopy (SEM) revealed species-specific yet fundamentally similar patterns of NFAP2-induced structural deterioration in *C. albicans* early-stage hyphae and *C. auris* pseudohyphae (Fig. 2). For *C. albicans*, the untreated filaments exhibited smooth, continuous surfaces characteristic of healthy polarized growth, whereas NFAP2 exposure typically resulted in a markedly altered topography, with heavily wrinkled and uneven surfaces and prominent globular protrusions that disrupted the native cylindrical contour. These fine-scale deformations are consistent with localized alterations in the cell envelope, which may reflect changes affecting the cell wall and underlying membrane, although the precise structural and mechanistic basis cannot be resolved based on SEM alone (Fig. 2A). A similar pattern was observed in *C. auris*, in which untreated pseudohyphae maintained an elongated morphology with smooth, cylindrical cell morphology. Following NFAP2 treatment, however, *C. auris* cells typically exhibited profound structural disintegration, including roughened, irregular surfaces, collapsed and wrinkled filaments, and regions of swelling or distortion. Localized ruptures, pronounced surface irregularities, and localized structural deformations were frequently observed. The normally well-defined hyphal tips became blunted, deformed, or collapsed, indicating disruption of the polarized extensions (Fig. 2B). Taken together, these morphological alterations indicate that NFAP2 exposure is associated with substantial disruption of cell envelope architecture in *C. albicans* and *C. auris*, albeit with species-specific manifestations, which may reflect membrane- and/or cell wall-associated effects, although a precise mechanism of action cannot be established from these data alone.

NFAP2 binding and uptake of early-stage filamentous *C. albicans* and pseudohyphal *C. auris* cells

The interaction and cellular uptake of boron-dipyrromethene–labeled NFAP2 (BODIPY-NFAP2; BD-NFAP2), a green fluorophore conjugate, were evaluated in early-stage filamentous *C. albicans* CBS 5982 and pseudohyphal *C. auris* NCPF 8971 cells by fluorescence microscopy. BD-NFAP2 was applied at sub-MIC concentrations (1.56 µg mL^{-1} for *C. albicans* and 3.12 µg mL^{-1} for *C. auris*), and the samples were analyzed after 10–120 min of incubation (Fig. 3).

For *C. albicans*, green fluorescence corresponding to BD-NFAP2 was detected as early as 30 min. It localized not only to the cell surface and hyphal tips but also to discrete intracellular foci, consistent with vacuolar compartments and possible endocytic trafficking. Between 45 and 60 min, the fluorescence intensity increased and became

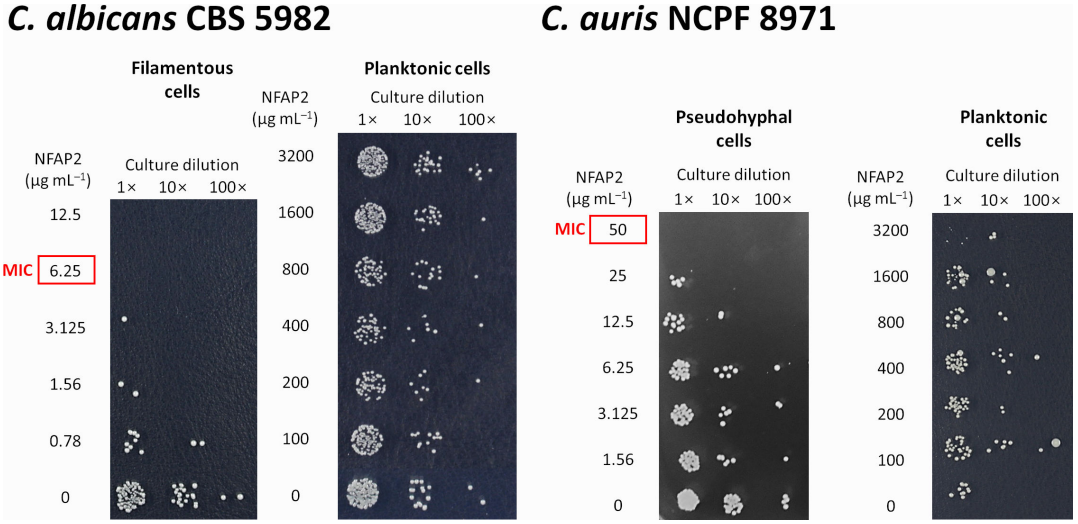

FIG 1 Filamentous *C. albicans* and pseudohyphal *C. auris* cells exhibit markedly higher susceptibility to NFAP2 compared with planktonic yeast forms. Spot assay analysis of early-stage filamentous *C. albicans* CBS 5982 (left) and pseudohyphal *C. auris* NCPF 8971 (right) after a 2-h NFAP2 exposure. Serial dilutions (1×, 10×, and 100×) of treated cultures were plated to assess colony formation. Filamentous *C. albicans* cells showed complete loss of detectable post-exposure viability at 6.25 μg mL^{-1} NFAP2, whereas planktonic cells remained unaffected even at 3,200 μg mL^{-1} under the tested conditions. Similarly, pseudohyphal *C. auris* cells showed complete loss of detectable post-exposure viability at 50 μg mL^{-1}, whereas planktonic cultures remained unaffected at concentrations up to 3,200 μg mL^{-1} under the tested conditions. This assay reflects short-term post-exposure viability following NFAP2 treatment rather than standard broth microdilution MIC determination. Apparent MIC values derived from the spot assay are summarized in the text for clarity. Red frames indicate the MIC values for filamentous *C. albicans* and pseudohyphal *C. auris*.

more evenly distributed along the hyphae, which indicated the progressive accumulation of NFAP2. Despite marked intracellular green fluorescence, the red propidium iodide (PI) staining remained primarily negative up to 60 min, suggesting that intracellular accumulation may occur prior to detectable membrane permeabilization, although this temporal sequence cannot be conclusively established from the current data. After 90 min, partial co-localization of green and red fluorescence was observed, suggesting that prolonged exposure results in membrane disruption and cell death (Fig. 3).

A similar time-dependent pattern was observed in *C. auris*. At 15 min, BD-NFAP2 fluorescence was faint and limited to the cell surface, with no detectable PI signal. After 30–45 min, marked intracellular fluorescence appeared, confirming NFAP2 internalization into pseudohyphal cells. At 60 min, fluorescence remained predominantly intracellular, with occasional minimal PI staining, consistent with largely preserved membrane integrity. This suggests that NFAP2 accumulation may occur prior to overt cell damage or death, although this relationship cannot be directly resolved from these observations.

Taken together, these results indicate that NFAP2 associates with and enters cells of *C. albicans* and *C. auris* during early exposure and accumulates intracellularly, whereas later stages are characterized by membrane-associated damage. However, the precise sequence and mechanism of these events cannot be conclusively determined. The early vacuolar localization in *C. albicans* is consistent with the possibility that endocytic trafficking may contribute to NFAP2 uptake, although this remains a hypothesis that requires direct experimental validation.

Transcriptomic changes of early-stage filamentous *C. albicans* cells under NFAP2 pressure

Transcriptomic analyses were performed at early exposure time points selected to minimize confounding effects of morphological reversion and later-stage adaptive responses, thereby capturing early NFAP2-associated cellular responses prior to overt membrane disruption (Fig. 3). Principal component analysis (PCA) demonstrated a clear separation between NFAP2-treated and untreated early-stage filamentous *C. albicans*

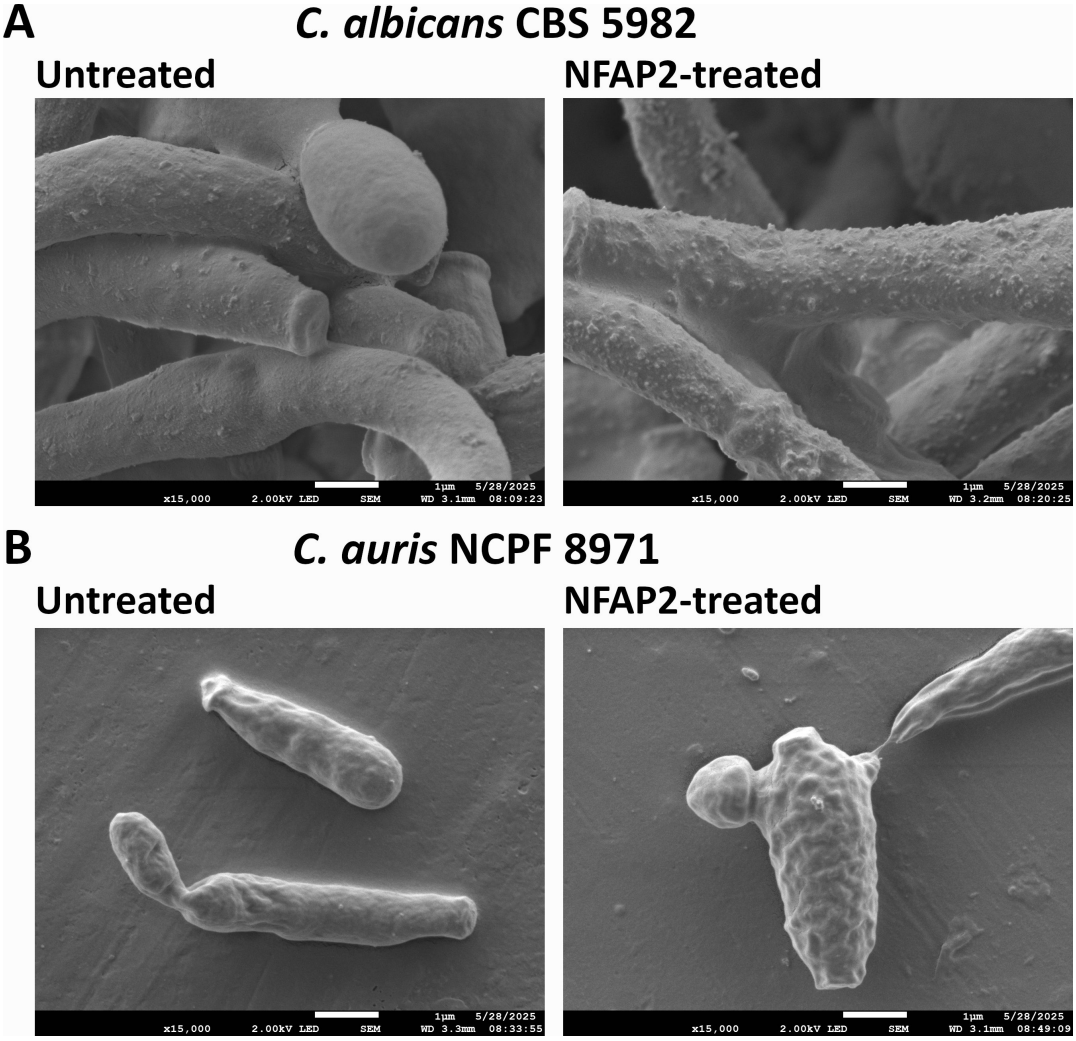

FIG 2 NFAP2 induces severe species-specific structural damage in early-stage filamentous *C. albicans* and pseudohyphal *C. auris* cells as determined by SEM. Early-stage filamentous *C. albicans* CBS 5982 and pseudohyphal *C. auris* NCPF 8971 cells were exposed to NFAP2 in LCM at 37°C under continuous shaking for 2 h. *C. albicans* cells were treated with 6.25 µg mL^{-1} NFAP2, whereas *C. auris* cells were treated with 50 µg mL^{-1} NFAP2 (apparent MIC values see Table S1). Untreated morphotype-matched cells served as controls. Untreated *C. albicans* early-stage hyphae display smooth, continuous surfaces characteristic of healthy polarized growth. In contrast, NFAP2-treated hyphae exhibit markedly altered surface architecture, including extensive wrinkling, uneven contours, and prominent globular protrusions, consistent with substantial cell envelope structural alterations that may reflect cell wall- and/or membrane-associated effects, although precise mechanisms cannot be resolved from SEM alone (A). Untreated *C. auris* pseudohyphae maintain elongated morphology with smooth surfaces, uniform diameter, and intact cell wall architecture. NFAP2 treatment is associated with profound structural deterioration, including roughened and irregular surfaces, collapsed and twisted filaments, swollen or distorted regions, and frequent localized ruptures with membrane extrusions. Hyphal tips appear blunted or deformed, reflecting disrupted polarized extension (B).

CBS 5982 samples, indicating a robust and reproducible transcriptomic response. PC1 explained the majority of the variation (68.83%) and distinctly segregated treated and untreated groups, whereas PC2 (13.29%) accounted for the minor intragroup variability without overlap (Fig. S3A). Consistently, a volcano plot displayed a substantial set of significantly regulated genes (adjusted $P < 0.05$; $\log_2$ fold-change (FC) > |1.5|) following NFAP2 treatment, including several markedly upregulated transcripts ($\log_2$FC > |3–4|) encoding core regulators of ribosome biogenesis, RNA processing, and translational capacity (Fig. S3B). Taken together, these analyses indicate pronounced and specific transcriptional changes associated with NFAP2 exposure in early-stage filamentous *C. albicans*, without establishing a direct causal relationship between NFAP2 activity and transcriptional reprogramming.

The upregulated transcripts were dominated by ribosome biogenesis and RNA metabolism, including essential nucleolar assembly factors (*RRP5*, *RIX1*, *IMP3*/*IMP4*, and *TSR1*), DEAD-box RNA helicases involved in rRNA maturation (*DED1*, *DBP2*, *DBP7*, and *DBP10*), and extensive sets of cytosolic and mitochondrial ribosomal proteins. Transcription factors associated with morphogenesis and metabolic control (*NDT80*, *SFL1*, and *SEF1*) were also induced, consistent with a strongly anabolic, ribosome-centered transcriptional profile rather than a classical antifungal stress response, without establishing that NFAP2 directly triggers this state (File S1). In contrast, the downregulated gene set was smaller but enriched in pathways that collectively reflect reduced adaptive flexibility and stress resilience (File S1). Key transcriptional regulators (*TLO4*/*8*/*10*, *RIM101*/pacC homolog, *SUT1*, *STD1*, *CSR1*, and *HAP42*) were suppressed, consistent with reduced environmental sensing, pH adaptation, and sterol remodeling capacity. Genes involved in nutrient acquisition and metabolic versatility, including *HGT17*/*19*, *HXK2*, *DUR3*, and *SMF1*, as well as lipid homeostasis factors, such as *RSB1*, *PGA10*, and *PGA42*, were also downregulated, suggesting a metabolic state that assumes nutrient abundance and deprioritizes scavenging and membrane maintenance. In addition, the repression of autophagy and membrane repair components (*ATG8*, *ATG101*, *PAC2*, and *YOP1*) and endocytic regulators (e.g., *VPS8*, *SNX3*, and YPT53) indicated a reduced capacity to clear or repair damaged cellular structures. Finally, multiple mitochondrial protection and redox-balancing genes (*PST1*, *PST3*, *POS5*, *CTA9*, *CTA26*, and HIG1-domain factors) were downregulated despite an increase in mitochondrial ribosomal gene expression, which may reflect a mismatch between mitochondrial biosynthesis and stress tolerance. File S1 illustrates how the upregulated and downregulated genes would be expected to contribute to NFAP2 sensitivity.

Functional enrichment analyses revealed that NFAP2 exposure is associated with distinct transcriptional responses in early-stage filamentous *C. albicans*, characterized by the activation of pathways involved in biosynthesis and gene expression rather than canonical stress- or proteostasis-associated programs. Gene Ontology (GO) Biological Process (BP) terms for the upregulated genes included macromolecule and organic substance biosynthesis, cellular nitrogen compound metabolism, gene expression, RNA processing, ncRNA metabolic processes, and ribosome biogenesis, indicating enhanced anabolic activity and increased translational capacity during early NFAP2 exposure. In contrast, downregulated BP terms were limited and primarily associated with cellular component organization, indicating only a modest reduction in structural or organizational functions (Fig. 4A).

Kyoto Encyclopedia of Genes and Genomes (KEGG) pathway analysis was consistent with the GO results, revealing significant upregulation of ribosome-associated pathways, including "Ribosome – *C. albicans*" and "Ribosome biogenesis in eukaryotes," consistent with increased translational capacity during early NFAP2 exposure rather than proteotoxic stress responses, without demonstrating that NFAP2 directly promotes this activation. Downregulated KEGG pathways included broad metabolic pathways and secondary metabolite biosynthesis, suggesting a shift away from energetically demanding specialized metabolic programs while maintaining core proliferative functions (Fig. 4B).

Molecular Function (MF) enrichment was restricted to upregulated genes and was dominated by RNA binding, structural molecule activity, and structural constituents of the ribosome, indicating enhanced engagement of the transcriptional and translational apparatus during early NFAP2 exposure (Fig. 5A). No MF terms were evident among the downregulated genes, suggesting that NFAP2 exerts limited functional repression at the level of molecular activities within this early developmental window.

GO Cellular Component (CC) analysis supported this transcriptional pattern. Upregulated genes were significantly enriched in ribonucleoprotein complexes, ribosomes, nucleolus, nuclear lumen, and various intracellular and organelle luminal compartments. These associations were consistent with increased RNA processing, ribosome assembly, and nucleus-associated biosynthetic functions (Fig. 5B). Consistent with the MF, no CC

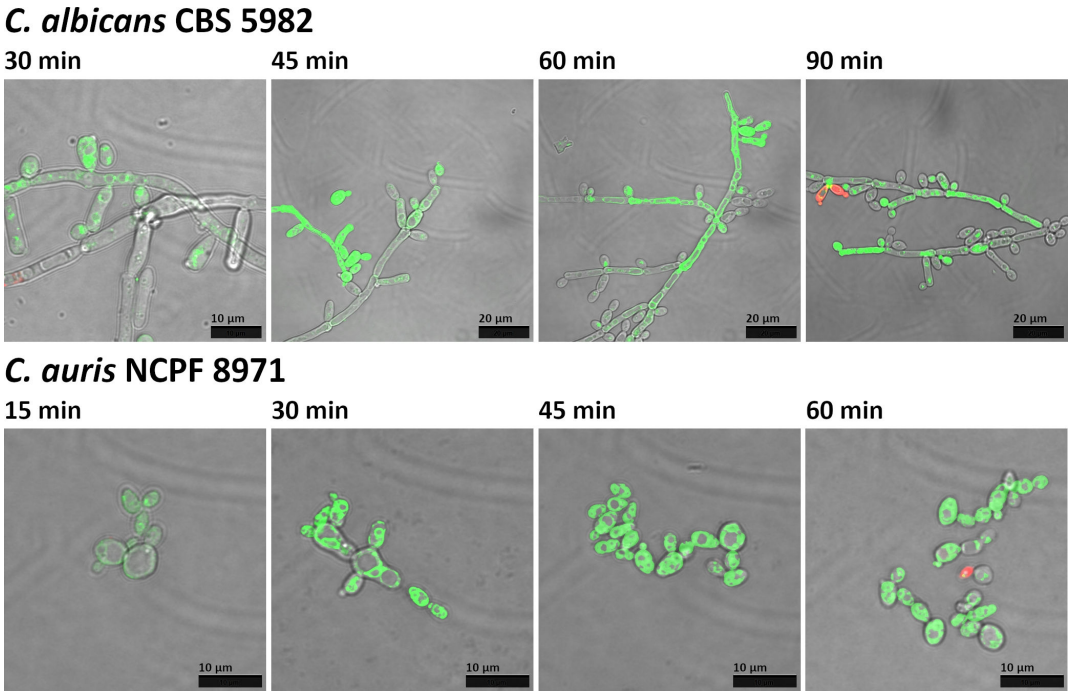

FIG 3 Time-dependent uptake of BODIPY (BD)-labeled NFAP2 in early-stage filamentous *C. albicans* and pseudohyphal *C. auris* cells. Fluorescence microscopy images showing the localization and intracellular accumulation of BD-NFAP2 (green) in early-stage filamentous *C. albicans* CBS 5982 (30–90 min) and pseudohyphal *C. auris* NCPF 8971 (15–60 min) cells treated with sub-MIC concentrations of 1.56 µg mL^{-1} and 3.12 µg mL^{-1}, respectively. In *C. albicans*, NFAP2 was detectable on the cell surface and within discrete intracellular foci by 30 min, followed by progressive, uniform intracellular accumulation at 45–60 min. PI staining (red) was detected only at 90 min, suggesting that intracellular accumulation may occur prior to membrane permeabilization, although this temporal sequence cannot be conclusively established. In *C. auris*, weak surface fluorescence was visible at 15 min, whereas marked intracellular fluorescence became detectable at 30–45 min. Only occasional PI-positive cells were detected at 60 min.

terms were enriched among the downregulated genes, suggesting that NFAP2 exposure is not associated with detectable suppression of specific cellular structures but is associated with selective enrichment of components involved in gene expression and ribosome biogenesis at this stage.

Taken together, these multilevel enrichment analyses indicate a coordinated transcriptional shift associated with NFAP2 exposure in early-stage filamentous *C. albicans*, characterized by the broad activation of biosynthetic, transcriptional, and ribosome-associated pathways. Rather than inducing classical stress-defense or proteostasis responses, NFAP2 exposure is associated with increased gene expression, RNA processing, and translational capacity, accompanied by reduced specialized metabolic functions, such as secondary metabolite biosynthesis. This pattern is consistent with the principal component analysis (PCA) and differential expression analyses and supports a working model in which an early anabolic, transcriptionally active state may be associated with NFAP2 susceptibility, without demonstrating that NFAP2 directly promotes this state.

Transcriptomic changes of pseudohyphal *C. auris* cells under NFAP2 pressure

Despite early sampling designed to capture primary responses, PCA revealed that the dominant source of variance in the *C. auris* transcriptomic data sets was sample-specific rather than treatment-specific (Fig. S4). For two experimental conditions corresponding to distinct NFAP2 concentrations (3.125 µg mL^{-1} and 25 µg mL^{-1}), treated samples were closely clustered with their corresponding untreated counterparts, forming clear sample pairs rather than treatment-defined groups. This indicates that intersample biological variability exceeds the transcriptional effect of NFAP2. Although small shifts between NFAP2-treated and untreated samples were visible within each pair, these differences

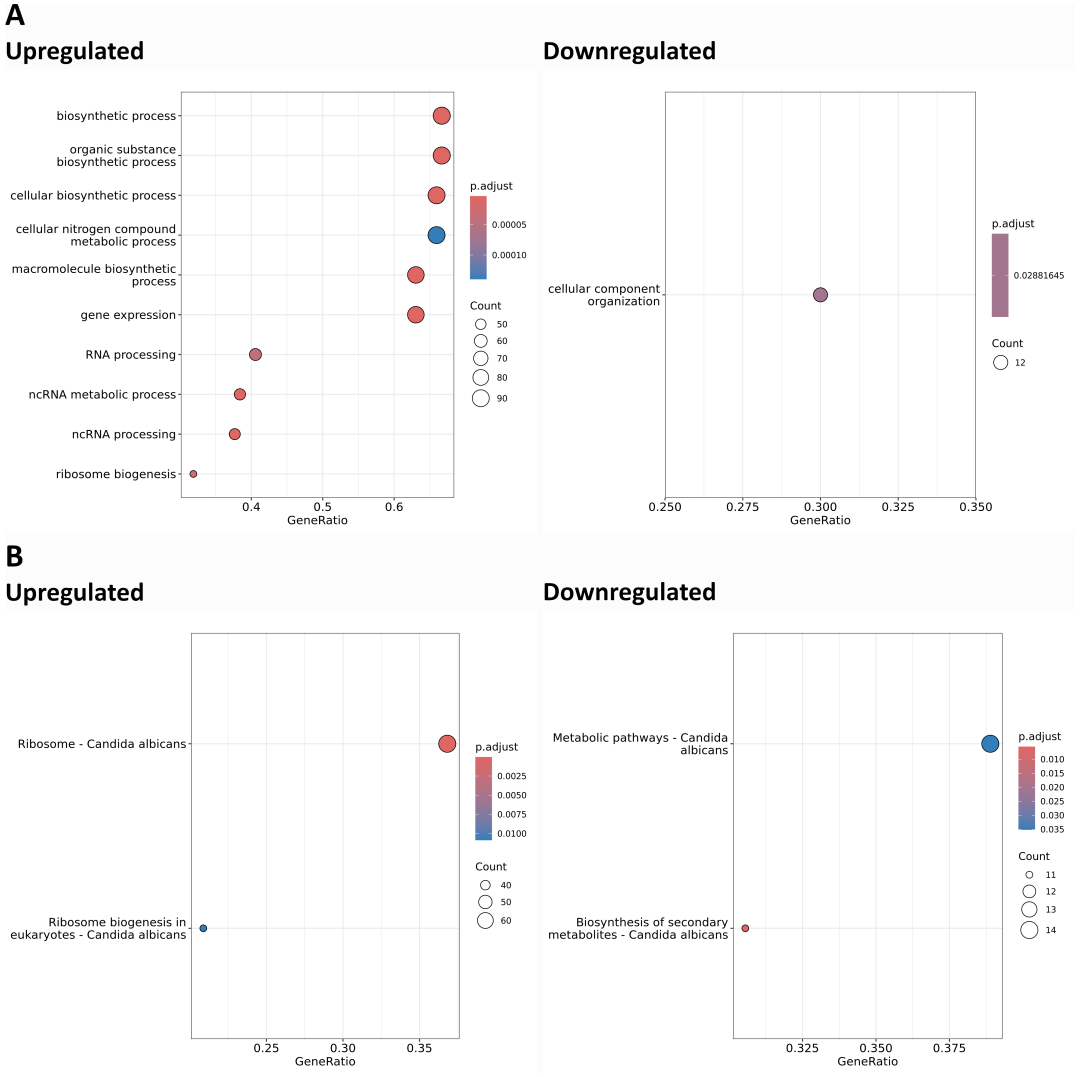

FIG 4 Functional enrichment analysis of NFAP2-responsive genes in early-stage filamentous *C. albicans* CBS 5982: Biological Process (BP) and Kyoto Encyclopedia of Genes and Genomes (KEGG) pathway. RNA-seq–based differential gene expression analysis was performed on NFAP2-treated and untreated morphotype-matched cells. Upregulated and downregulated gene sets were defined using thresholds of $\log_2$ fold-change ≥ |1.5| and adjusted *P* value < 0.05. Gene Ontology (GO) Biological Process (BP) and KEGG pathway enrichment analyses were conducted using clusterProfiler (26). GO BP enrichment of upregulated and downregulated genes (A). Upregulated genes were predominantly enriched in biosynthetic and gene expression–related processes, including macromolecule biosynthesis, cellular nitrogen compound metabolism, RNA processing, ncRNA metabolism, gene expression, and ribosome biogenesis. In contrast, downregulated genes showed limited enrichment, with a single significant term related to cellular component organization. KEGG pathway enrichment of upregulated and downregulated genes (B). Upregulated pathways were dominated by ribosome-associated categories, including "Ribosome – *C. albicans*" and "Ribosome biogenesis in eukaryotes." Downregulated pathways included broader metabolic categories, such as general metabolic pathways and secondary metabolite biosynthesis. Dotplots display significantly enriched GO and KEGG terms (adjusted *P* < 0.05). Dot size represents gene count, and color indicates adjusted *P* value.

were subtle and did not drive the global separation of the treated and untreated groups along PC1 or PC2.

Consistent with this pattern, a volcano plot analysis revealed no statistically significant gene-level transcriptional changes under either condition (Fig. S5). No genes met the combined significance and effect sizes threshold required to qualify as differentially expressed after multiple-testing correction. This absence of differentially expressed genes across both low- (3.125 µg mL^{-1}) and high-dose (25 µg mL^{-1}) NFAP2 exposures indicates that pseudohyphal *C. auris* does not undergo robust, detectable transcriptional reprogramming under the applied conditions (Fig. S4 and S5).

The overall shape of the volcano plots was similar across conditions, with scattered fold-change outliers and a complete absence of significantly up- or downregulated genes. Together with the paired PCA structure, these results indicate that NFAP2 exposure is not associated with a robust transcriptional stress response in *C. auris*. Instead, the observed effects were weak and diffuse, falling below the threshold of detection for gene-specific differential expression. This contrasts with the strong transcriptional responses observed in *C. albicans* and is consistent with the possibility that *C. auris* may rely primarily on non-transcriptional or post-transcriptional mechanisms to tolerate antifungal stress, although this interpretation remains hypothesis-driven.

Evaluation of the toxicity and therapeutic effect of NFAP2 in the *Galleria mellonella* larval infection model

To determine whether NFAP2 is safe and therapeutically effective against filamentous *Candida* in a whole-organ context, we used the *Galleria mellonella* larval infection model for *in vivo* toxicity and survival assays.

Survival analysis in *G. mellonella* larvae indicated that NFAP2 did not induce dose-dependent toxicity. The survival curves largely overlapped with the untreated control across all tested concentrations, indicating that NFAP2 is well tolerated. No evidence of acute or cumulative toxicity was observed, which supports the safety of NFAP2 for *in vivo* antifungal applications (Fig. 6A).

For the *G. mellonella*–filamentous *C. albicans* infection model, NFAP2 treatment not only failed to improve survival but also significantly worsened larval mortality relative to the *C. albicans*-infected, untreated group ($P < 0.0001$) (Fig. 6B). In contrast, NFAP2 exerted a moderate ($0.005 < P < 0.05$) but transient survival benefit in pseudohyphal *C. auris*-infected larvae, with partial early protection that decreased over time. This opposing, species- and morphotype-dependent effect highlights the fundamentally different *in vivo* susceptibilities to NFAP2. File S2 provides a statistical analysis of the toxicity and therapeutic efficacy of NFAP2 in the *G. mellonella* larval infection model.

DISCUSSION

From a methodological perspective, the use of aerated, shaken liquid cultures to generate homogeneous early-stage filamentous *C. albicans* and pseudohyphal *C. auris* populations represents a practical approach for studying morphotype-specific antifungal susceptibility, particularly in emerging multidrug-resistant pathogens, such as *C. auris* (6, 27). In contrast to static biofilm models, this approach eliminates extracellular matrix interference and nutrient stratification while providing highly synchronized, morphologically stable populations that are suitable for MIC testing, rapid pharmacodynamic measurements, and downstream omics. The observed approximate 2-h window of filament and pseudohypha stability is consistent with the well-established dynamic plasticity of *Candida* morphogenesis (5, 28). Moreover, the stable, elongated pseudohyphal form of *C. auris* that we generated is in line with reports identifying filamentation as an inducible and clinically relevant phenotype (8) (Fig. S2). This narrow and reproducible interval is well suited for interrogating fast-acting AFPs, such as NFAP2, before morphotype reversion alters its susceptibility(7). However, this experimental setup does not recapitulate extracellular matrix-associated biofilm conditions, which may influence antifungal susceptibility and transcriptional responses (29). While this reductionist system improves morphotype synchronization and enables mechanistic dissection of early NFAP2 susceptibility, it does not fully capture the complex extracellular matrix barriers, nutrient gradients, altered diffusion dynamics, or biofilm-specific adaptive programs that characterize mature *Candida* biofilms in clinical settings. Consequently, the observed NFAP2 susceptibility patterns may differ quantitatively or mechanistically under true biofilm conditions, and future studies should directly evaluate NFAP2 activity within extracellular matrix-rich biofilm architectures. Accordingly, findings from this model should be interpreted cautiously when extrapolating to broader therapeutic optimization.

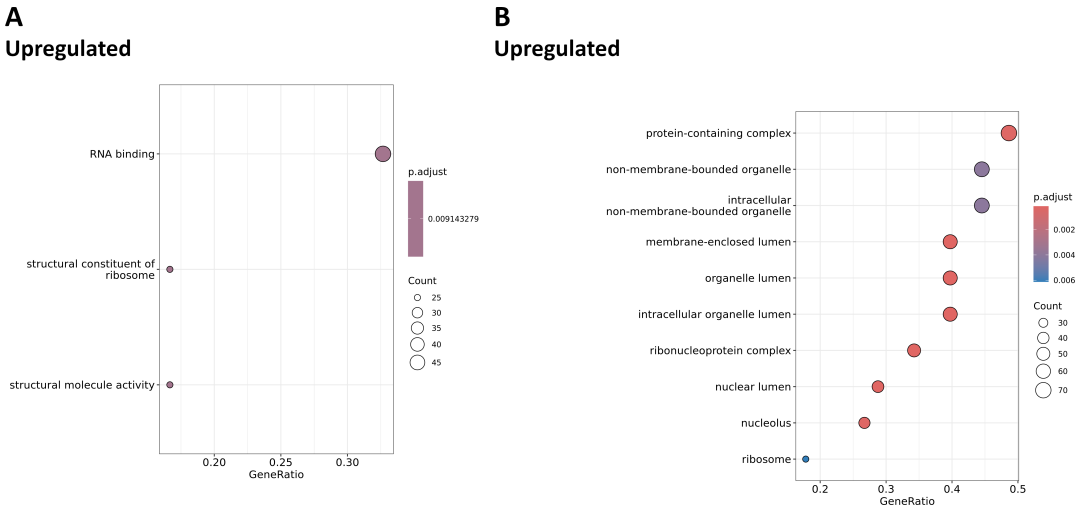

FIG 5 Functional enrichment analysis of NFAP2-responsive genes in early-stage filamentous *C. albicans* CBS 5982: Molecular Function (MF) and Cellular Component (CC). RNA-seq–based differential gene expression analysis was performed on NFAP2-treated and untreated morphotype-matched cells. Upregulated and downregulated gene sets were defined using thresholds of $\log_2$ fold-change ≥ |1.5| and adjusted *P* value < 0.05. Gene Ontology (GO) Molecular Function (MF) and Cellular Component (CC) enrichment analyses were conducted using clusterProfiler (26). GO MF enrichment of upregulated genes (A). Upregulated genes were enriched for RNA binding, structural molecule activity, and ribosomal structural components. No significantly enriched MF terms were detected among the downregulated genes. GO CC enrichment of upregulated genes (B). Upregulated genes were associated with protein-containing complexes, ribonucleoprotein complexes, ribosomes, the nucleolus, nuclear lumen, and organelle luminal compartments. No significantly enriched CC terms were detected among the downregulated genes. Dotplots display significantly enriched GO terms (adjusted *P* < 0.05). Dot size represents gene count, and color indicates adjusted *P* value.

A key finding of the present study is that early morphogenesis creates a transient physiological vulnerability for both species (Fig. 1). Importantly, we note that comparisons between planktonic and early morphogenetic states inherently involve distinct physiological baselines and culture histories. Therefore, the observed differences in NFAP2 susceptibility cannot be attributed solely to morphotype but may also reflect differences in metabolic state, prior growth conditions, and medium adaptation. Although filamentation generally enhances virulence and environmental resilience (7, 8), early-stage filamentous cells exhibited increased sensitivity to NFAP2 under the applied experimental conditions (Fig. 1). This aligns with the concept that early morphogenetic states represent highly active developmental phases characterized by intensive cell wall remodeling, high energetic and biosynthetic demand, and increased permeability and protein uptake (4, 9, 10), which may collectively contribute to NFAP2 sensitivity. Therefore, increased susceptibility may reflect not morphology alone but a broader growth-associated physiological vulnerability.

Fluorescent imaging with BD-NFAP2 supports a multistep NFAP2 interaction pattern. Early internalization may occur prior to detectable membrane permeabilization (Fig. 3), which is in line with the known mechanisms of other disulfide-stabilized AFPs, in which non-lytic uptake occurs before intracellular disruption (30–36). This apparent kinetic separation of entry and membrane damage is consistent with the observed time-dependent killing patterns and differentiates NFAP2 from conventional cell wall-active antifungals, such as the echinocandins (5, 15), which inhibit membrane-localized β-1,3-glucan synthase but primarily disrupt fungal cell wall biosynthesis rather than directly destabilizing the plasma membrane. These results are based on a post-exposure viability assay rather than standard broth microdilution MIC determination and therefore reflect short-term susceptibility following NFAP2 treatment.

Ultrastructural analyses reveal severe NFAP2-induced cell envelope damage in both species, with species-specific manifestations. In *C. albicans*, NFAP2 is associated with the formation of globular protrusions and localized surface wrinkling, consistent with early

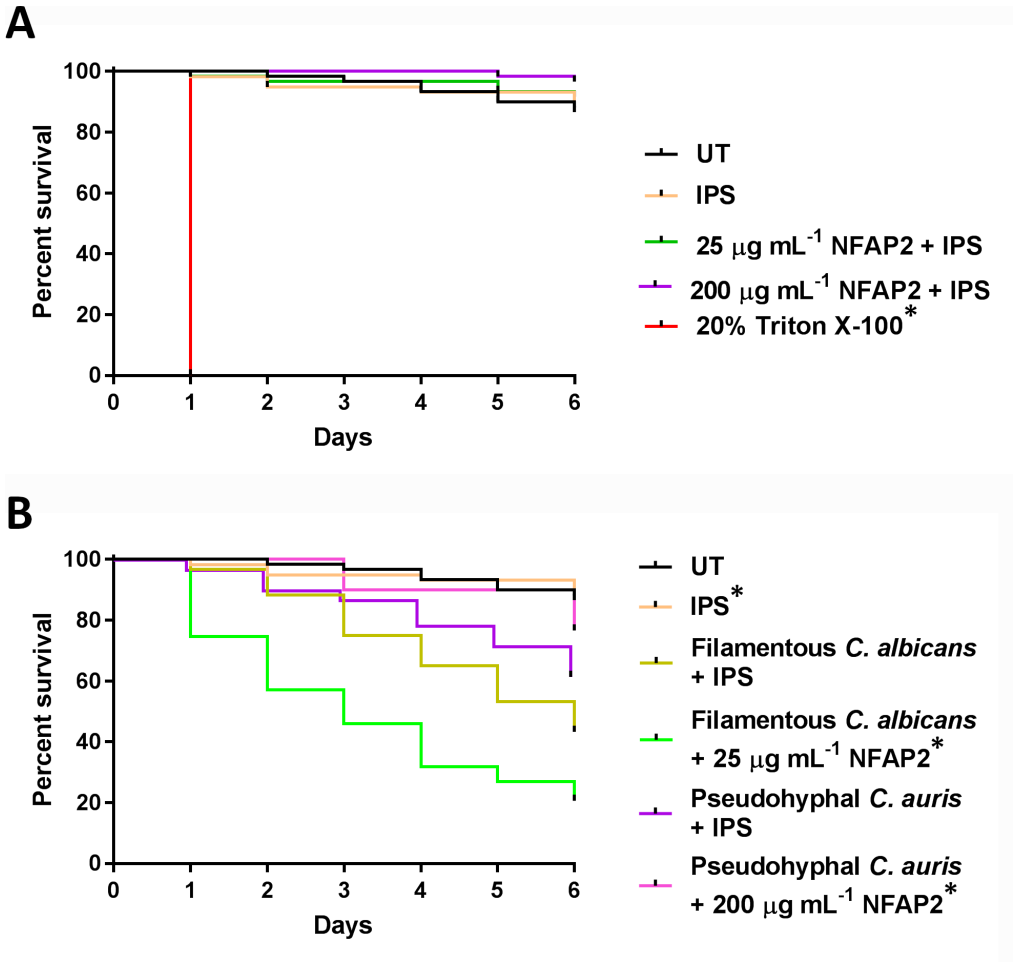

FIG 6 *In vivo* safety and therapeutic efficacy of NFAP2 in *G. mellonella* larvae. NFAP2-treated uninfected larvae exhibited survival rates comparable to those of untreated controls for all tested doses, indicating the absence of dose-dependent or cumulative toxicity (A). In infected larvae, NFAP2 did not improve survival in the filamentous *C. albicans* CBS 5982 infection model and was associated with worsened outcome, whereas a moderate and transient protective effect was observed in the pseudohyphal *C. auris* NCPF 8971 infection model (B). IPS, insect physiological saline-treated control; UT, untreated control. *$P \leq 0.05$ by both log-rank (Mantel–Cox) and Gehan–Breslow–Wilcoxon tests compared with the infected (*C. albicans* or *C. auris* + IPS), untreated group. Triton X-100 (20% [vol/vol]) was used as a positive toxicity control. Taken together, these results indicate that NFAP2 is well tolerated *in vivo* but exhibits strongly species- and morphotype-dependent therapeutic effects.

membrane reorganization and wall weakening, whereas *C. auris* pseudohyphae exhibit dramatic collapse, twisting, swelling, and ruptures accompanied by membrane extrusions (Fig. 2). These morphological features support the profound deficits in wall rigidity, turgor maintenance, and polarized growth. Similar cell envelope perturbation and severe structural collapse have been documented for other AFPs, including *Penicillium chrysogenum* PAF and PAFB (32–34), as well as *Aspergillus giganteus* AFP, which disrupts chitin synthesis and weakens wall architecture (37). *C. auris* showed the most dramatic NFAP2-induced damage, which is consistent with SEM studies indicating that sertraline produces comparable surface irregularities and membrane disruption (38), as well as with reports of new small molecules targeting *C. auris* biofilms that induce similar cell wall and plasma membrane damage (39–41). Taken together, these data are consistent with a model in which NFAP2 appears to interact with the fungal cell envelope through multiple phases, including surface interaction, early destabilization, and ultimately catastrophic structural failure, although the precise sequence and mechanism cannot be conclusively established.

Transcriptomic analyses further illuminate the vulnerability of *C. albicans* (Fig. 4 and 5). NFAP2-treated early filamentous *C. albicans* is characterized by a hyper-anabolic transcriptomic profile, as evidenced by the upregulation of macromolecule biosynthesis, RNA processing, ncRNA metabolism, ribosome assembly, rRNA-processing helicases, ribosomal proteins, and nucleolar components, which are hallmarks of a heightened transcriptional and translational program reported under hypha-inducing conditions and linked to ribosome biogenesis, rRNA processing, and nucleolar functions (42). The induction of morphogenetic regulators, such as *SFL1* (signaling repression of hyphal development), *NDT80* (a component of morphogenetic/biofilm regulatory circuits), and *SEF1* (virulence regulator under host-relevant conditions), reinforces the interpretation that NFAP2-exposed cells maintain active growth/morphogenesis programs rather than entering a canonical general stress response (43–45). In contrast, downregulated genes highlight the targeted collapse of adaptive flexibility. Although broad deregulation of core canonical glucan or chitin biosynthetic genes was not detected, NFAP2 exposure was associated with reduced expression of several genes linked to cell envelope maintenance, cell wall integrity signaling, pH-dependent wall remodeling, GPI-anchored cell surface proteins, glycoprotein processing, vesicle trafficking, and membrane–cell wall homeostasis, including RIM101/RIM21, PGA10/PGA42, DPM3, MNS1, FMP45, CSR1, HOF1, ECM21, VPS8, SNX3, YPT53, RSB1, SUT1, ARE2, and ERG4. These transcriptional trends suggest suppression of adaptive cell envelope maintenance programs rather than uniform shutdown of canonical glucan/chitin biosynthesis, although targeted pathway-level validation remains necessary for definitive mechanistic resolution. Reduced expression of regulators governing environmental sensing, carbon-source utilization, sterol remodeling, and pH adaptation (*TLO4/8/10*, *RIM101*/pacC homolog, *SUT1*, *STD1*, *CSR1*, *and HAP42*) is consistent with a physiological shift prioritizing biosynthesis at the expense of stress resilience (46–48). The concomitant suppression of nutrient uptake, lipid homeostasis, autophagy, and membrane repair factors, together with mismatched mitochondrial remodeling (e.g., changes in the expression of organelle-linked genes), indicates a high-load, instability-prone state, which agrees with the broad transcriptome reprogramming observed in *Candida albicans* during environmental changes (49, 50).

These patterns align with the broader literature on the multiphase mechanisms of AFPs in *C. albicans*. NFAP2 is a potent anti-*Candida* protein with well-established structural determinants and anti-biofilm activity (23, 51). Its dual mode of action (membrane disruption at the MIC and intracellular targeting at the sub-MIC) is consistent with the multiphase characteristics of the present study (24). The early time point analyzed here likely precedes the long-term NFAP2-associated metabolic suppression described in planktonic *C. albicans* (24), which may explain the predominance of transcriptional and ribosomal activation over extensive stress signatures. Direct comparison with previously published planktonic NFAP2 transcriptomic data sets, including long-term sub-MIC exposure models, remains inherently limited due to major differences in morphotype, developmental state, cultivation media, NFAP2 exposure duration, and experimental design (24). Consequently, such data sets cannot reliably resolve the specific regulatory architecture of early morphogenetic NFAP2 susceptibility observed here. Future matched-condition comparative transcriptomic studies will therefore be required to enable a more rigorous mechanistic dissection. Notably, our results differ from transcriptomic responses induced by other AFPs, such as MAF-1A, which induce oxidative stress and metabolic arrest (52); however, ribosome biogenesis signatures in fungi are not exclusively growth markers. They can also accompany adaptive restructuring under stress, as observed in butanol-treated *C. albicans* (53). The strong enrichment of RNA processing, ribosome assembly, and nucleolar categories reflects a dynamic reconfiguration during early NFAP2 exposure rather than the absence of stress. This is consistent with emerging evidence that post-transcriptional regulation, including P-body factors (54) and chromatin modulators, such as SAGA (55), is central to morphological transitions. Taken together, these results support a multistep model of NFAP2 activity, in which NFAP2 exposure coincides with a transcriptional state

characterized by growth-associated transcriptional programs, suppression of adaptive pathways, and delayed membrane destabilization (25, 56).

NFAP2 appears to be associated with impaired antifungal defense responses. Repression of MDR1, an azole efflux pump essential for fluconazole tolerance (57, 58), is consistent with reduced drug resistance. ERG4, SUT1, and ARE2 downregulation disrupts sterol homeostasis (59, 60). The suppression of RIM101/RIM21 impairs pH-dependent wall remodeling (61). Decreased RSB1, SNX3, YOP1, and the α-arrestin adaptor ECM21, along with reduced RSN1 and the endoplasmic reticulum–associated degradation lectin YOS9, compromise lipid homeostasis, vesicle trafficking, stress-gated ion homeostasis, and endoplasmic reticulum protein-quality control, all of which shape azole and amphotericin B susceptibility (62–66). Concurrent downregulation of mitochondrial detoxification genes (*PST1*/*3*, *POS5*, and *CTA9*/*26*) and proteostasis regulators (*ATG8* and *PAC2*), along with reduced nutrient-uptake systems (*HGT17*/*19*, *HXK2*, and *DUR3*), further reduces the capacity of cells to maintain redox balance, membrane integrity, and metabolic stability under stress conditions (67–72). Although NFAP2 exposure coincides with limited compensatory upregulation of *ERG25*, *FLU1*, *PHO84*/*87*, *GCS1*, *IPT1*, *SHO1*, and *SIT1* (73–75), these partial responses are not sufficient to offset the extensive deficits in membrane stability, efflux capacity, mitochondrial detoxification, and proteostasis (76–79). Overall, NFAP2 exposure corresponds to an early hyphal state characterized by weakened membrane and wall integrity, reduced stress resilience, and disrupted metabolic flexibility. The combined suppression of resistance-associated pathways and limited compensatory responses may help explain the previously observed synergy of NFAP2 with conventional antifungals against planktonic and filamentous morphotypes (22, 23, 50).

Importantly, these observations may support a systems-level interpretation in which early morphogenetic states represent transient physiological configurations characterized by elevated biosynthetic activity and reduced stress resilience (80). In this context, increased anabolic and translational activity may coincide with reduced buffering capacity against environmental perturbations, thereby creating a temporally restricted window of vulnerability. However, this interpretation remains hypothetical and requires direct experimental validation.

Although early filamentous and pseudohyphal morphologies remained morphologically stable during the experimental window, metabolic and transcriptional adaptation to LCM likely occurred in parallel. We note that transferring cells from species-specific filamentation media into low-cation LCM may itself alter the transcriptional and metabolic landscape of both *C. albicans* and C. *auris*, even in the absence of NFAP2. Therefore, the transcriptional changes observed in this study should be interpreted as NFAP2-associated responses within an LCM exposure context rather than as medium-independent NFAP2-specific effects. This limitation cannot be fully separated within the current experimental design and will require dedicated medium-control transcriptomic comparisons in future studies (81).

In *C. auris*, PCA did not reveal a treatment-driven separation but instead indicated sample-specific variation as the primary source of variance, and no significantly regulated genes were identified. These findings suggest that NFAP2 exposure is associated with only subtle, low-amplitude transcriptional shifts (Fig. S4 and S5). Discrepancies between multivariate clustering and gene-level significance are well documented and may reflect coordinated microchanges across many transcripts that alter global variance structure without producing marked differential expression (82, 83). This pattern supports the possibility that *C. auris* may rely on post-transcriptional or non-transcriptional regulatory buffering mechanisms rather than robust transcriptional reprogramming during antifungal stress response. However, given the limited number of biological replicates, sample-specific variability, and potential constraints in statistical power, alternative explanations, including distributed low-amplitude transcriptional responses or experimental variance, cannot be excluded. Compared with *C. albicans*, this species often exhibits muted transcriptional responses to antifungal stimuli (84–87).

Accordingly, the PCA-derived separation may reflect widespread but shallow transcriptomic adjustments rather than discrete regulatory responses. Overall, the primary robust finding is the absence of statistically significant gene-level differential expression under the applied thresholds, whereas mechanistic interpretations should be considered hypothesis-generating.

We further acknowledge that differences in morphotype architecture between *C. albicans* hyphae and *C. auris* pseudohyphae may partially contribute to the divergent transcriptional responses observed here (27, 28) (Fig. S3–S5). Accordingly, the present findings should be interpreted within the specific species–morphotype contexts examined rather than as universally generalizable morphotype-specific transcriptional programs. Expanded within-species analyses across additional morphotypes will therefore be necessary for more rigorous mechanistic resolution.

The absence of NFAP2-associated toxicity in *G. mellonella* agrees with previous studies showing that antifungal proteins and their γ-core–derived peptides exhibit high selectivity for fungal cells while sparing host tissues (Fig. 6A) (88). This supports the use of NFAP2 for *in vivo* applications and is consistent with studies showing that *G. mellonella* serves as a practical intermediate model to detect compound toxicity, evaluate antifungal efficacy, and support prioritization before vertebrate testing (89–91). In the filamentous *C. albicans* infection model, however, NFAP2 did not have a therapeutic benefit. Instead, it significantly worsened larval survival relative to the IPS control (Fig. 6B), indicating that morphotype-specific *in vitro* vulnerability does not necessarily translate into improved host outcome for all infections. This unexpected worsening of survival in the filamentous *C. albicans* infection model represents a notable biological observation that requires careful consideration. Possible explanations include suboptimal dosing or timing, high inoculum burden, morphotype-specific host–pathogen interactions, or stress-induced modulation of fungal virulence under sublethal NFAP2 exposure. However, the current experimental design does not allow discrimination among these possibilities. Future studies incorporating fungal burden measurements, histopathology, and host-response analyses will be required to resolve the underlying mechanisms. This unexpected outcome suggests that, under certain infection contexts, peptide exposure may alter host–pathogen dynamics in a manner not captured by *in vitro* susceptibility alone. Notably, untreated filamentous *C. albicans* caused substantially greater larval mortality than pseudohyphal *C. auris* (Fig. 6B), indicating important baseline species-specific differences in virulence under the applied infection conditions. This higher intrinsic pathogenicity may have reduced the effective therapeutic window for NFAP2 intervention in *C. albicans* and should therefore be considered when interpreting species-dependent differences in treatment efficacy. Sublethal antifungal stress has been reported to modulate *C. albicans* virulence-associated traits, supporting the possibility that dosing, timing, or morphotype-specific physiology can shift *in vivo* outcomes and should be addressed by follow-up burden and host-response readouts (92, 93). In contrast, NFAP2 provided a moderate but transient survival advantage in the pseudohyphal *C. auris* model (Fig. 6B), which is consistent with a species- and morphotype-dependent efficacy profile. In addition, the ionic and biochemical composition of host hemolymph may variably modulate NFAP2 activity through ionic shielding, altered peptide stability, or reduced bioavailability, potentially contributing to species-, morphotype-, or regimen-dependent differences in therapeutic efficacy. The limited and short-lived protection in *C. auris* indicates its pronounced phenotypic variability and regulatory plasticity (94), as well as its documented capacity to evade or suppress host immune effector functions compared with *C. albicans* (95, 96). Because only a single post-infection treatment regimen was evaluated, dose–response relationships and timing-dependent therapeutic effects remain to be determined. Taken together, these results place NFAP2, under the tested experimental conditions, within the broader class of membrane-active antifungal proteins/peptides, whose activity and therapeutic performance are strongly contingent on fungal developmental state and host–pathogen context, which highlights the need for species- and regimen-specific

optimization. Accordingly, the translational implications of these findings should be interpreted cautiously and considered preliminary, pending further validation under expanded experimental conditions.

Conclusion

This study revealed that the early morphogenetic transitions in the tested *C. albicans* and *C. auris* strain are associated with increased NFAP2 susceptibility. Using a rapid and standardized cultivation platform, we showed that NFAP2 exhibits increased antifungal activity against early-stage hyphae and pseudohyphae, highlighting transient developmental states as periods of enhanced antifungal vulnerability. In *C. albicans*, transcriptomic and network analyses indicate an anabolic, translation-associated gene expression signature accompanied by the suppression of various stress-protective pathways. This pattern is consistent with a working model in which anabolic transcriptional activity and reduced stress-adaptive capacity may contribute to the increased fragility of emerging hyphae, although this causal relationship remains to be directly validated (Fig. 7). In *C. auris*, increased susceptibility of pseudohyphal cells occurred without detectable transcriptional remodeling, consistent with a response profile in which NFAP2 sensitivity may be influenced by biophysical, non-transcriptional, or post-transcriptional determinants rather than large-scale transcriptional reprogramming. Importantly, the *in vivo* data revealed species- and morphotype-dependent effects: NFAP2 conferred a moderate but transient survival benefit in *G. mellonella* infected with pseudohyphal *C. auris*, whereas no survival advantage—and a worsened outcome—was observed in the filamentous *C. albicans* model. Together, these findings provide a proof-of-concept framework for understanding morphotype-associated susceptibility to peptide- and protein-based antifungal strategies and support future validation across broader strain, species, and therapeutic contexts.

MATERIALS AND METHODS

Strains and media

C. albicans CBS 5982 and *C. auris* NCPF 8971 strains were maintained on yeast extract–peptone–dextrose (YPD) agar slants (yeast extract 10 g L^{-1}, peptone 20 g L^{-1}, glucose 20 g L^{-1}, and agar 20 g L^{-1}) at 4°C. AIM V Medium (research grade; Thermo Fisher Scientific, Waltham, MA, USA) and an optimized FIM (glucose 0.5 g L^{-1}, yeast extract 0.25 g L^{-1}, peptone 0.125 g L^{-1}, and NaCl 2.5 g L^{-1}) were used to induce filamentation in *C. albicans* and *C. auris*, respectively. Species-specific filamentation-inducing media were selected because *C. albicans* and *C. auris* possess substantially different morphogenetic induction requirements, and preliminary optimization identified AIM V and FIM as the most reproducible conditions for generating homogeneous early-stage filamentous and pseudohyphal populations, respectively. The morphological stability of early-stage filamentous *C. albicans* and pseudohyphal *C. auris* cells was evaluated in a low-cation medium (LCM; glucose 5 g L^{-1}, yeast extract 0.25 g L^{-1}, and peptone 0.125 g L^{-1}), which was used consistently across all NFAP2 exposure and antifungal susceptibility assays to minimize ionic shielding effects, medium-dependent variability, thereby enhancing the activity of NFAP2.

NFAP2 production

Recombinant NFAP2 (~100% purity) was produced using a *P. chrysogenum*–based expression system and was purified as previously described (21, 48).

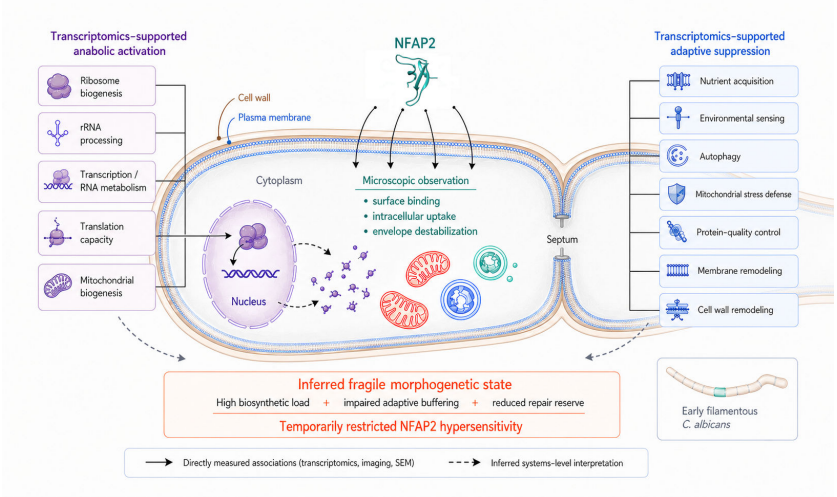

FIG 7 Integrated working model of experimentally supported observations and inferred processes associated with increased NFAP2 susceptibility in early-stage filamentous *C. albicans*. Early filamentation is associated with a transcriptional state characterized by elevated ribosome biogenesis, rRNA processing, RNA metabolism, transcriptional activity, translation-associated functions, and mitochondrial biosynthetic programs (left), as determined by RNA-seq, differential gene expression, and functional enrichment analyses, and integrated with microscopy-based observations. Concurrently, multiple adaptive and stress-protective pathways are relatively suppressed (right), including nutrient acquisition, environmental sensing, autophagy, mitochondrial stress responses, protein-quality control, membrane remodeling, and cell wall remodeling. These experimentally supported transcriptional features are consistent with a transient physiological configuration in which increased anabolic activity coincides with reduced adaptive buffering capacity. NFAP2 (center), a membrane-active antifungal protein, is associated with early cellular binding, intracellular accumulation, and pronounced structural alterations in this morphotype, as supported by fluorescence imaging and SEM analyses. Together, these observations are consistent with a working model in which early morphogenetic states may represent a vulnerable physiological window associated with increased NFAP2 susceptibility. Solid elements indicate experimentally measured observations, whereas dashed elements represent inferred or hypothetical relationships that require further direct validation. In the color scheme used for the cell interior, purple denotes components of the transcriptional machinery and RNA metabolism, orange marks the mitochondria, green highlights elements of the autophagy and vesicular trafficking pathways, and blue identifies other intracellular compartments and quality-control systems. Elements of this schematic figure were generated with the assistance of ChatGPT 5.3 (OpenAI) and were subsequently manually edited, finalized, and scientifically validated by the authors.

Generation and isolation of early-stage filamentous and pseudohyphal *Candida* cells

Mid-log phase *C. albicans* cells were grown in YPD, and *C. auris* cells (2×10^5 cells mL^{-1}) were grown in LCM at 30°C overnight with continuous shaking (160 rpm). Cells were inoculated into 5 mL AIM V (*C. albicans*) and 5 mL FIM (*C. auris*) medium in 15 mL centrifuge tubes and incubated at 37°C for 16 (*C. albicans*) or 18 h (*C. auris*) with shaking at 180 rpm. Early-stage filamentous cells were operationally defined as elongated, non-branching hyphal or pseudohyphal forms observed prior to extensive network formation or morphological maturation. After incubation, early-stage filamentous *C. albicans* cells were separated from planktonic cells. The aggregates and fully developed filaments were removed using a 70 µm pore size cell strainer (VWR Cell Strainer; Avantor, Radnor, PA, USA). Early-stage filaments were subsequently isolated from the remaining planktonic cells using a second filtration step with a 40 µm pore size strainer (VWR Cell Strainer; Avantor, Radnor, PA, USA). The retained filaments were washed from the filter surface with LCM, and this filtration–washing step was repeated

once. Filtration was not required for *C. auris*, as >90% of the cells displayed pseudohyphal morphology under these conditions.

The morphological stability of early-stage filamentous *C. albicans* and pseudohyphal *C. auris* cells (2×10^5 cells mL^{-1}) was evaluated in 5 mL LCM at 37°C with shaking at 180 rpm. Filamentation and reversion processes were monitored using an Olympus BX53 light microscope equipped with an Olympus XC50 digital camera. The enrichment of early-stage filamentous and pseudohyphal populations was verified microscopically based on established morphological criteria (elongation, septation, and absence of mature hyphal branching), which were applied consistently across all experiments, although no quantitative morphometric analysis was performed.

NFAP2 susceptibility testing

Susceptibility assays were performed exclusively in LCM to standardize NFAP2 activity measurements and minimize medium-dependent ionic interference. Early-stage filamentous *C. albicans* and pseudohyphal *C. auris* cells were subjected to susceptibility testing under these standardized conditions. *Candida* cells (1×10^5 cells mL^{-1}) were exposed to 0.78–12.5 µg mL^{-1} of NFAP2 (*C. albicans*) or 12.5–200 µg mL^{-1} of NFAP2 (*C. auris*) in LCM at 37°C for 2 h under continuous shaking (400 rpm). The cells were washed twice with LCM (7,800 × *g*, 5 min). Five-microliter drops of 10-fold serial dilutions of each NFAP2 treatment were spotted onto LCM agar plates (LCM supplemented with 20 g L^{-1} agar) and incubated at 37°C for 48 h. The minimum inhibitory concentration (MIC) was defined as the lowest NFAP2 concentration for which no colonies appeared on the agar surface. One loop (10 µL) of planktonic control cells was pre-cultured under standard yeast-form growth conditions in LCM at 37°C for 16 h under continuous shaking (160 rpm) to reach the mid-log growth phase prior to susceptibility testing. Cells were counted using a Bürker chamber and standardized to an inoculum density of 1×10^5 cells mL^{-1} before NFAP2 exposure to match filamentous susceptibility assay conditions. Untreated cells served as negative controls. Susceptibility tests were conducted in three independent biological replicates. This assay reflects post-exposure viability rather than standard broth microdilution MIC values and therefore should be interpreted as a short-term viability-based susceptibility measure.

SEM

Early-stage filamentous *C. albicans* and pseudohyphal *C. auris* cells (1×10^5) were treated with 6.25 µg mL^{-1} and 50 µg mL^{-1} of NFAP2, respectively, as described above for the NFAP2 susceptibility assays. Untreated cells served as the morphological controls. *Candida* cells were harvested (7,800 × *g*, 5 min), washed twice with phosphate-buffered saline (PBS), and resuspended in PBS. Aliquots (8 µL) were spotted onto silicon disks that were coated with 0.01% (wt/vo) poly-L-lysine (Merck Millipore, Billerica, MA, USA). The samples were fixed overnight at 4°C in 2.5% (vol/vol) glutaraldehyde and 0.05 M cacodylate buffer (pH 7.2) prepared in PBS. After two PBS washes, the samples were dehydrated in a graded ethanol series (30%, 50%, 70%, 80%, 96%, and 100% [vol/vol], each for 24 h at 4°C). The samples were then incubated in a graded series of the chemical drying agent hexamethyldisilazane (33%, 50%, and 66%, each for 1 h at room temperature, 100% [vol/vol] for 2 h, diluted in absolute ethanol), sputter-coated with 12 nm gold, and analyzed using a JEOL JSM-7100F/LV field-emission scanning electron microscope (JEOL Ltd., Tokyo, Japan).

NFAP2-binding/internalization

BD-NFAP2 was used to assess the localization of NFAP2 in early-stage filamentous *C. albicans* and pseudohyphal *C. auris* cells. In *C. auris* experiments, unlabeled NFAP2 was co-applied with BODIPY FL EDA (Invitrogen, Waltham, MA, USA)-conjugated NFAP2 to maintain the intended total NFAP2 exposure while keeping fluorescence signal intensity within an interpretable range. This approach ensured sufficient peptide exposure for measurable biological interaction under *C. auris* susceptibility conditions while

preventing excessive fluorescence intensity and potential detector saturation during imaging. Filtered early-stage filamentous *C. albicans* cells (2×10^7 cells mL^{-1}) were treated with 1.56 µg mL^{-1} of BD-NFAP2, whereas twice-washed (2,400 × *g*, 5 min) pseudohyphal *C. auris* cells (2×10^7 cells mL^{-1}) were exposed to a mixture of 1.56 µg mL^{-1} NFAP2 and 1.56 µg mL^{-1} BD-NFAP2 in LCM. The treatments were conducted for 15, 30, 45, 60, and 90 min at 37°C with continuous shaking at 400 rpm. Following incubation, the cells were washed with phosphate-buffered saline (PBS, pH 7.4; 7,800 × *g*, 5 min) and stained with 5 µg mL^{-1} PI (Sigma-Aldrich, St. Louis, MO, USA) for 10 min at room temperature in the dark. After two PBS washes (7,800 × *g*, 5 min), the samples were resuspended in PBS and analyzed using a confocal laser-scanning microscope (Olympus Fluoview FV1000; Olympus, Shinjuku, Japan) with a 488 nm excitation laser. The excitation/emission settings were 504/512 nm for BD-NFAP2 and 535/617 nm for PI. Sequential scanning was performed to prevent spectral crosstalk between fluorophores.

RNA isolation and sequencing

Sampling time points were selected to capture early transcriptional responses prior to extensive morphological reversion or secondary adaptive changes. These time points were further guided by uptake and membrane integrity kinetics (Fig. 3), indicating that NFAP2 internalization occurs within 30-60 min, whereas detectable membrane permeabilization emerges at later stages. Early-stage filamentous *C. albicans* cells (~2×10^7 mL^{-1}) were incubated with 1.56 µg mL^{-1} NFAP2 in LCM for 60 min at 37°C under continuous shaking (400 rpm) in four independent experiments, whereas pseudohyphal *C. auris* cells (~2×10^8 mL^{-1}) were exposed to 3.125 µg mL^{-1} NFAP2 for 45 min or to 25 µg mL^{-1} under the same conditions in three and four independent experiments, respectively. The parallel RNA-seq experiments at low (3.125 µg mL^{-1}) and high (25 µg mL^{-1}) NFAP2 concentrations were designed to assess whether the absence of detectable transcriptional responses reflected insufficient peptide exposure or rapid high-dose cellular damage. Untreated morphotype-matched biological replicates served as transcriptomic controls for all RNA sequencing experiments.

For total RNA isolation, early-stage filamentous *C. albicans* cells were thawed, refrozen in liquid nitrogen, and resuspended in lysis buffer in bashing lysis tubes, followed by mechanical disruption using a Tissuelyser LT (Qiagen) for 20 min at 50 Hz. The *C. auris* pseudohyphae were ground for 1 min with nuclease-free sand using a microcentrifuge tube–compatible glass pestle. They were frozen again in liquid nitrogen and reground in lysis buffer. The lysates were centrifuged at 9,000 × *g* for 2 min. Total RNA was purified using the Quick-RNA Plant Miniprep Kit (Zymo Research, Tustin, CA, USA) based on the manufacturer's instructions. RNA quantity and purity were assessed using a NanoDrop ND-1000 spectrophotometer (Thermo Fisher Scientific, Waltham, MA, USA). Total RNA samples were sequenced (6 Gb raw data per sample) by Novogene GmbH (Munich, Germany) using the NovaSeq X Plus Series PE150 platform (Illumina, San Diego, CA, USA).

Transcriptome analysis

Quality assessment of the reads was performed using FastQC 0.12.1 (https://github.com/s-andrews/FastQC). Raw reads were quality trimmed with Trimmomatic 0.39 (97) using the following parameters: SLIDINGWINDOW:4:20 MINLEN:100. STAR 2.7.11b aligner (98) was used with default settings to map the quality-filtered reads on *C. albicans* SC5314 (GCF_000182965.3) or *C. auris* B11220 (GCF_003013715.1) reference genomes. The read counts covering all of the genes were calculated using featureCounts of Rsubread 2.16.1 (99). The differentially expressed genes were called by DESeq2 version 1.42.1 (83). The threshold values for DEG calling were set to $\log_2$ fold-change ≥ |1.5| and adjusted *P* value < 0.05. GO enrichment analysis (100, 101) and Kyoto KEGG pathway enrichment analysis (102) were conducted using the enrichGO and enrichKEGG functions of the clusterProfiler 4.10.1 R package (26). For GO enrichment analysis, a custom *C. albicans* OrgDb annotation package was created using the makeOrgPackageFromNCBI function of the AnnotationForge 1.44.0 R package (https://bioconductor.org/packages/

AnnotationForge) using taxID:5476. AnnotationDbi 1.64.1 R package (https://bioconductor.org/packages/AnnotationDbi) was used to query the generated OrgDb. For KEGG enrichment, the enrichKEGG function was used with the parameter organism = 'cal'. Enriched GO terms and KEGG pathways were considered significant based on a false discovery rate (FDR)-corrected $P < 0.05$. The plots were created with ggplot2 3.5.1 (103), EnhancedVolcano 1.20.0 (https://bioconductor.org/packages/EnhancedVolcano), and enrichplot 1.22.0 R packages (https://bioconductor.org/packages/enrichplot). The R version was 4.3.3 (2024-02-29) with Bioconductor version 3.18. Differential expression analyses were performed relative to untreated, morphotype-matched controls using standardized quality-control filtering, normalization, and statistical significance thresholds.

Galleria mellonella infection model assays

G. mellonella larvae (final instar stage, 250–300 mg) were used to evaluate the *in vivo* antifungal efficacy of NFAP2. The larvae were maintained at 30°C in the dark; however, before experimentation, they were incubated at 37°C in the dark. For infection, groups of 20 larvae were injected with 20 µL of a standardized suspension of early-stage filamentous *C. albicans* CBS 5982 or pseudohyphal *C. auris* NCPF 8971 cells (2×10^7 cells mL^{-1}) into the last left proleg using a Hamilton syringe. Post-infection, 10 µL of NFAP2 was administered into the same proleg at defined concentrations (200 µg mL^{-1} for *C. albicans* and 25 µg mL^{-1} for *C. auris*). Larvae injected with 20 µL IPS (20% vol/vol), larvae treated with NFAP2 alone (200 µg mL^{-1}), and 20% (vol/vol) Triton X-100–treated larvae served as nontoxic, NFAP2 toxicity, and positive toxicity controls, respectively. The untreated larvae served as negative controls. Larval survival was monitored at 24-h intervals for up to 6 days.

To assess *G. mellonella* survival, statistical analyses were performed using the log-rank (Mantel–Cox) test and the Gehan–Breslow–Wilcoxon test in GraphPad Prism 7.00 (GraphPad Software, Boston, MA, USA). Differences in survival were considered significant when $P \leq 0.05$ in both tests. All survival analyses were conducted using GraphPad Prism 7.00 software (GraphPad Software, Boston, MA, USA).

ACKNOWLEDGMENTS

The present work of L.G. was supported by the Hungarian National Research, Development and Innovation Office – NKFIH, K 146131. Open-access publication was supported by the University of Szeged Open Access Fund (Grant ID: 8344).

AUTHOR AFFILIATIONS

[1]Department of Biotechnology and Microbiology, Faculty of Science and Informatics, University of Szeged, Szeged, Hungary
[2]Doctoral School of Biology, Faculty of Science and Informatics, University of Szeged, Szeged, Hungary
[3]Institute of Plant Biology, HUN-REN Biological Research Centre, Szeged, Hungary
[4]Department of Theoretical Health Sciences and Health Management, Faculty of Health Sciences and Social Studies, University of Szeged, Szeged, Hungary
[5]Department of Genetics, Faculty of Science and Informatics, University of Szeged, Szeged, Hungary

AUTHOR ORCIDs

Gábor Bende http://orcid.org/0000-0003-4571-9775
László Galgóczy http://orcid.org/0000-0002-6976-8910

FUNDING

Funder	Grant(s)	Author(s)
Nemzeti Kutatási Fejlesztési és Innovációs Hivatal	K 146131	László Galgóczy
Szegedi Tudományegyetem	OA 8344	László Galgóczy

AUTHOR CONTRIBUTIONS

Richárd Merber, Formal analysis, Investigation, Methodology, Validation, Visualization, Writing – original draft, Writing – review and editing | Krisztián Laczi, Data curation, Formal analysis, Investigation, Validation, Visualization, Writing – original draft | Gábor Bende, Formal analysis, Investigation, Methodology, Visualization | Erika Kazinczi, Formal analysis, Investigation | Attila Farkas, Investigation, Methodology, Visualization | Gergely Maróti, Methodology, Resources, Writing – original draft, Writing – review and editing | Rita Sinka, Formal analysis, Methodology, Resources, Writing – original draft, Writing – review and editing | László Galgóczy, Conceptualization, Formal analysis, Funding acquisition, Methodology, Project administration, Resources, Supervision, Validation, Visualization, Writing – original draft, Writing – review and editing

DATA AVAILABILITY

The raw sequencing reads and read-count data were deposited in the NCBI Gene Expression Omnibus database under accession number (GSE316902) (104).

ADDITIONAL FILES

The following material is available online.

Supplemental Material

File S1 (Spectrum00404-26-S0001.xlsx). Up- and down-regulated genes in response to NFAP2 in early-stage filamentous *Candida albicans* CBS 5982.
File S2 (Spectrum00404-26-S0002.xlsx). Statistical analysis of the toxicity and therapeutic efficacy of NFAP2 in the *Galleria mellonella* larval infection model.
Table S1 and Figures S1 to S5 (Spectrum00404-26-S0003.pdf). Table S1: Summary of apparent MIC values demonstrating morphotype-dependent susceptibility of *Candida albicans* CBS 5982 and *Candidozyma auris* NCPF 8971 to NFAP2. Fig. S1: Generation of early-stage filamentous *C. albicans* and pseudohyphal *C. auris* cells under optimized liquid culture conditions. Fig. S2: Morphological stability of early-stage filamentous C. albicans and pseudohyphal C. auris cells in LCM medium at 37°C. Fig. S3: Global transcriptomic response of early-stage filamentous *C. albicans* CBS 5982 to NFAP2 treatment. Fig. S4: Principal component analysis (PCA) of NFAP2-treated (CaurT) and untreated (CaurU) *C. auris* samples under two NFAP2 concentration conditions. Fig. S5: Volcano plots of NFAP2-treated versus untreated *C. auris* samples under two NFAP2 concentration conditions.

Open Peer Review

PEER REVIEW HISTORY (review-history.pdf). An accounting of the reviewer comments and feedback.

REFERENCES

1. World health organization. 2022. WHO fungal priority pathogens list to guide research, development and public health action. Geneva: World Health Organization.
2. Centers for Disease Control and Prevention (US). 2024. Tracking *Candida auris*: United States, 2024 update. CDC, Atlanta, GA.
3. LymanM, ForsbergK, SextonDJ, ChowNA, LockhartSR, Jackson BR, ChillerT. 2023. Worsening spread of *Candida auris* in the United States. MMWR Morb Mortal Wkly Rep 72:293–298. https://doi.org/10.7326/M22-3469
4. Parambath S, Dao A, Kim HY, Zawahir S, Izquierdo AA, Tacconelli E, Govender N, Oladele R, Colombo A, Sorrell T, Ramon-Pardo P, Fusire T, Gigante V, Sati H, Morrissey CO, Alffenaar JW, Beardsley J. 2024. *Candida albicans*-a systematic review to inform the World Health

Organization fungal priority pathogens list. Med Mycol 62:myae045. https://doi.org/10.1093/mmy/myae045
5. Eix EF, Nett JE. 2025. *Candida auris*: epidemiology and antifungal strategy. Annu Rev Med 76:57–67. https://doi.org/10.1146/annurev-med-061523-021233
6. Hayes JF. 2024. *Candida auris*: epidemiology update and a review of strategies to prevent spread. J Clin Med 13:6675. https://doi.org/10.3390/jcm13226675
7. Brandquist ND, Lampman C, Smith EJ, Basilio L, Almansob A, Iwen PC, Blankenship JR. 2023. Significant variation of filamentation phenotypes in clinical *Candida albicans* strains. Front Cell Infect Microbiol 13:1207083. https://doi.org/10.3389/fcimb.2023.1207083
8. Fan S, Yue H, Zheng Q, Bing J, Tian S, Chen J, Ennis CL, Nobile CJ, Huang G, Du H. 2021. Filamentous growth is a general feature of *Candida auris* clinical isolates. Med Mycol 59:734–740. https://doi.org/10.1093/mmy/myaa116
9. Fan F, Liu Y, Liu Y, Lv R, Sun W, Ding W, Cai Y, Li W, Liu X, Qu W. 2022. *Candida albicans* biofilms: antifungal resistance, immune evasion, and emerging therapeutic strategies. Int J Antimicrob Agents 60:106673. https://doi.org/10.1016/j.ijantimicag.2022.106673
10. Kaur J, Nobile CJ. 2023. Antifungal drug-resistance mechanisms in *Candida biofilms*. Curr Opin Microbiol 71:102237. https://doi.org/10.1016/j.mib.2022.102237
11. Mannan M, Nabeela S, Mishra R, Uppuluri P. 2024. Host immune response against fungal biofilms. Curr Opin Microbiol 81:102520. https://doi.org/10.1016/j.mib.2024.102520
12. Silva S, Rodrigues CF, Araújo D, Rodrigues ME, Henriques M. 2017. *Candida* species biofilms' antifungal resistance. J Fungi (Basel) 3:8. https://doi.org/10.3390/jof3010008
13. Cavalheiro M, Teixeira MC. 2018. *Candida* biofilms: threats, challenges, and promising strategies. Front Med (Lausanne) 5:28. https://doi.org/10.3389/fmed.2018.00028
14. Spivak ES, Hanson KE. 2018. *Candida auris*: an emerging fungal pathogen. J Clin Microbiol 56:e01588-17. https://doi.org/10.1128/JCM.01588-17
15. Ajetunmobi OH, Badali H, Romo JA, Ramage G, Lopez-Ribot JL. 2023. Antifungal therapy of *Candida biofilms*: past, present and future. Biofilm 5:100126. https://doi.org/10.1016/j.bioflm.2023.100126
16. U.S. Food & drug administration (FDA). 2023. Rezafungin (Rezzayo) label information. Silver Spring, MD
17. Oshiro KGN, Rodrigues G, Monges BED, Cardoso MH, Franco OL. 2019. Bioactive peptides against fungal biofilms. Front Microbiol 10:2169. https://doi.org/10.3389/fmicb.2019.02169
18. Kissmann AK, Mildenberger V, Krämer M, Alpízar-Pedraza D, Martell-Huguet EM, Perez-Erviti JA, Cetinkaya A, Pietrasik J, Otero-Gonzalez AJ, Firacative C, Rodríguez A, Ständker L, Weil T, Stenger S, Rosenau F. 2025. Anti-biofilm peptides can rescue fluconazole and amphotericin b efficacies against *Candida albicans*. Sci Rep 15:24593. https://doi.org/10.1038/s41598-025-10315-4
19. Fernández de Ullivarri M, Arbulu S, Garcia-Gutierrez E, Cotter PD. 2020. Antifungal peptides as therapeutic agents. Front Cell Infect Microbiol 10:105. https://doi.org/10.3389/fcimb.2020.00105
20. Robbins N, Caplan T, Cowen LE. 2017. Molecular evolution of antifungal drug resistance. Annu Rev Microbiol 71:753–775. https://doi.org/10.1146/annurev-micro-030117-020345
21. Tóth L, Kele Z, Borics A, Nagy LG, Váradi G, Virágh M, Takó M, Vágvölgyi C, Galgóczy L. 2016. NFAP2, a novel cysteine-rich anti-yeast protein from *Neosartorya fischeri* NRRL 181: isolation and characterization. AMB Express 6:75. https://doi.org/10.1186/s13568-016-0250-8
22. Kovács R, Holzknecht J, Hargitai Z, Papp C, Farkas A, Borics A, Tóth L, Váradi G, Tóth GK, Kovács I, Dubrac S, Majoros L, Marx F, Galgóczy L. 2019. *In vivo* applicability of *Neosartorya fischeri* antifungal protein 2 (NFAP2) in treatment of vulvovaginal candidiasis. Antimicrob Agents Chemother 63:18–e01777. https://doi.org/10.1128/AAC.01777-18
23. Kovács R, Nagy F, Tóth Z, Forgács L, Tóth L, Váradi G, Tóth GK, Vadászi K, Borman AM, Majoros L, Galgóczy L. 2021. The *Neosartorya fischeri* antifungal protein 2 (NFAP2): a new potential weapon against multidrug-resistant *Candida auris* biofilms. Int J Mol Sci 22:771. https://doi.org/10.3390/ijms22020771
24. Dán K, Zsindely N, Kele Z, Laczi K, Karemera JK, Papp C, Farkas A, Maróti G, Borics A, Bodai L, Galgóczy L. 2025. Beyond plasma membrane disruption: novel antifungal mechanism of *Neosartorya (Aspergillus) fischeri* antifungal protein 2 in *Candida albicans*. Int J Biol Macromol 327:146558. https://doi.org/10.1016/j.ijbiomac.2025.146558
25. Bende G, Zsindely N, Laczi K, Kristóffy Z, Papp C, Farkas A, Tóth L, Sáringer S, Bodai L, Rákhely G, Marx F, Galgóczy L. 2025. The *Neosartorya (Aspergillus) fischeri* antifungal protein NFAP2 has low potential to trigger resistance development in *Candida albicans in vitro*. Microbiol Spectr 13(1):e0127324. https://doi.org/10.1128/spectrum.01273-24
26. Wu T, Hu E, Xu S, Chen M, Guo P, Dai Z, Feng T, Zhou L, Tang W, Zhan L, Fu X, Liu S, Bo X, Yu G. 2021. clusterProfiler 4.0: a universal enrichment tool for interpreting omics data. Innovation (Camb) 2:100141. https://doi.org/10.1016/j.xinn.2021.100141
27. De Gaetano S, Midiri A, Mancuso G, Avola MG, Biondo C. 2024. *Candida auris* outbreaks: current status and future perspectives. Microorganisms 12(5):927. https://doi.org/10.3390/microorganisms12050927
28. Wakade RS, Wellington M, Krysan DJ. 2024. Temporal dynamics of *Candida albicans* morphogenesis and gene expression reveals distinctions between *in vitro* and *in vivo* filamentation. mSphere 9:e0011024. https://doi.org/10.1128/msphere.00110-24
29. Finkel JS, Mitchell AP. 2011. Genetic control of *Candida albicans* biofilm development. Nat Rev Microbiol 9:109–118. https://doi.org/10.1038/nrmicro2475
30. Struyfs C, Cammue BPA, Thevissen K. 2021. Membrane-interacting antifungal peptides. Front Cell Dev Biol 9:649875. https://doi.org/10.3389/fcell.2021.649875
31. Oberparleiter C, Kaiserer L, Haas H, Ladurner P, Andratsch M, Marx F. 2003. Active internalization of the *Penicillium chrysogenum* antifungal protein PAF in sensitive aspergilli. Antimicrob Agents Chemother 47:3598–3601. https://doi.org/10.1128/AAC.47.11.3598-3601.2003
32. Leiter E, Szappanos H, Oberparleiter C, Kaiserer L, Csernoch L, Pusztahelyi T, Emri T, Pócsi I, Salvenmoser W, Marx F. 2005. Antifungal protein PAF severely affects the integrity of the plasma membrane of *Aspergillus nidulans* and induces an apoptosis-like phenotype. Antimicrob Agents Chemother 49:2445–2453. https://doi.org/10.1128/AAC.49.6.2445-2453.2005
33. Marx F, Binder U, Leiter E, Pócsi I. 2008. The *Penicillium chrysogenum* antifungal protein PAF, a promising tool for the development of new antifungal therapies and fungal cell biology studies. Cell Mol Life Sci 65:445–454. https://doi.org/10.1007/s00018-007-7364-8
34. Huber A, Galgóczy L, Váradi G, Holzknecht J, Kakar A, Malanovic N, Leber R, Koch J, Keller MA, Batta G, Tóth GK, Marx F. 2020. Two small, cysteine-rich and cationic antifungal proteins from *Penicillium chrysogenum*: a comparative study of PAF and PAFB. Biochim Biophys Acta Biomembr 1862:183246. https://doi.org/10.1016/j.bbamem.2020.183246
35. Garrigues S, Gandía M, Popa C, Borics A, Marx F, Coca M, Marcos JF, Manzanares P. 2017. Efficient production and characterization of the novel and highly active antifungal protein AfpB from *Penicillium digitatum*. Sci Rep 7:14663. https://doi.org/10.1038/s41598-017-15277-w
36. Hajdu D, Huber A, Czajlik A, Tóth L, Kele Z, Kocsubé S, Fizil Á, Marx F, Galgóczy L, Batta G. 2019. Solution structure and novel insights into phylogeny and mode of action of the *Neosartorya (Aspergillus) fischeri* antifungal protein (NFAP). Int J Biol Macromol 129:511–522. https://doi.org/10.1016/j.ijbiomac.2019.02.016
37. Hagen S, Marx F, Ram AF, Meyer V. 2007. The antifungal protein AFP from *Aspergillus giganteus* inhibits chitin synthesis in sensitive fungi. Appl Environ Microbiol 73:2128–2134. https://doi.org/10.1128/AEM.02497-06
38. Gowri M, Jayashree B, Jeyakanthan J, Girija EK. 2020. Sertraline as a promising antifungal agent: inhibition of growth and biofilm of *Candida auris* with special focus on the mechanism of action *in vitro*. J Appl Microbiol 128:426–437. https://doi.org/10.1111/jam.14490
39. Lara HH, Ixtepan-Turrent L, Jose Yacaman M, Lopez-Ribot J. 2020. Inhibition of *Candida auris* biofilm formation on medical and environmental surfaces by silver nanoparticles. ACS Appl Mater Interfaces 12:21183–21191. https://doi.org/10.1021/acsami.9b20708
40. Zeng H, Stadler M, Abraham WR, Müsken M, Schrey H. 2023. Inhibitory effects of the fungal pigment rubiginosin c on hyphal and biofilm formation in *Candida albicans* and *Candida auris*. J Fungi (Basel) 9:726. https://doi.org/10.3390/jof9070726
41. Parveen H, Mukhtar S, Albalawi MO, Khasim S, Ahmad A, Wani MY. 2024. Concomitant Inhibition and collaring of dual-species biofilms formed by *Candida auris* and *Staphylococcus aureus* by triazole based small molecule inhibitors. Pharmaceutics 16:1570. https://doi.org/10.3390/pharmaceutics16121570

42. Tebbji F, Chen Y, Richard Albert J, Gunsalus KTW, Kumamoto CA, Nantel A, Sellam A, Whiteway M. 2014. A functional portrait of Med7 and the mediator complex in *Candida albicans*. PLoS Genet 10:e1004770. https://doi.org/10.1371/journal.pgen.1004770
43. Li Y, Su C, Mao X, Cao F, Chen J. 2007. Roles of *Candida albicans* Sfl1 in hyphal development. Eukaryot Cell 6:2112–2121. https://doi.org/10.1128/EC.00199-07
44. Nobile CJ, Johnson AD. 2015. *Candida albicans* biofilms and human disease. Annu Rev Microbiol 69:71–92. https://doi.org/10.1146/annurev-micro-091014-104330
45. Chen C, Noble SM. 2012. Post-transcriptional regulation of the Sef1 transcription factor controls the virulence of *Candida albicans* in its mammalian host. PLoS Pathog 8:e1002956. https://doi.org/10.1371/journal.ppat.1002956
46. Bensen ES, Martin SJ, Li M, Berman J, Davis DA. 2004. Transcriptional profiling in Candida albicans reveals new adaptive responses to extracellular pH and functions for Rim101p. Mol Microbiol 54:1335–1351. https://doi.org/10.1111/j.1365-2958.2004.04350.x
47. Cottier F, Tan AS, Chen J, Lum J, Zolezzi F, Poidinger M, Pavelka N. 2015. The transcriptional stress response of *Candida albicans* to weak organic acids. G3 (Bethesda) 5(4):497–505. https://doi.org/10.1534/g3.114.015941
48. Huang G. 2012. Regulation of phenotypic transitions in the fungal pathogen *Candida albicans*. Virulence 3:251–261. https://doi.org/10.4161/viru.20010
49. Bruno VM, Wang Z, Marjani SL, Euskirchen GM, Martin J, Sherlock G, Snyder M. 2010. Comprehensive annotation of the transcriptome of the human fungal pathogen *Candida albicans* using RNA-seq. Genome Res 20:1451–1458. https://doi.org/10.1101/gr.109553.110
50. Hromatka BS, Noble SM, Johnson AD. 2005. Transcriptional response of *Candida albicans* to nitric oxide and the role of the YHB1 gene in nitrosative stress and virulence. Mol Biol Cell 16:4814–4826. https://doi.org/10.1091/mbc.e05-05-0435
51. Tóth L, Váradi G, Borics A, Batta G, Kele Z, Vendrinszky Á, Tóth R, Ficze H, Tóth GK, Vágvölgyi C, Marx F, Galgóczy L. 2018. Anti-candidal activity and functional mapping of recombinant and synthetic *Neosartorya fischeri* antifungal protein 2 (NFAP2). Front Microbiol 9:393. https://doi.org/10.3389/fmicb.2018.00393
52. Wang T, Xiu J, Zhang Y, Wu J, Ma X, Wang Y, Guo G, Shang X. 2017. Transcriptional responses of *Candida albicans* to Antimicrobial Peptide MAF-1A. Front Microbiol 8:894. https://doi.org/10.3389/fmicb.2017.00894
53. Anand R, Birke R, Martinez P, Delbrel E, Lamas-Berkley S, Bachellier-Bassi S, d'Enfert C, Papon N, Trieu-Cuot P, Munro CA, Brown AJP. 2023. Reprogramming in *Candida albicans* gene expression during butanol stress: Non-coding RNA metabolism, ribosome biogenesis and metabolic remodeling. Int J Mol Sci 24. https://doi.org/10.3390/ijms242417227
54. Tosiano MA, Bergmann A, Haynes BC, Noble SM, Erwig LP, Lorenz MC. 2025. Roles of P-body factors in *Candida albicans* filamentation and pathogenesis. PLoS Genet 21(1):e1011632. https://doi.org/10.1371/journal.pgen.1011632
55. Rashid S, Correia-Mesquita TO, Godoy P, Omran RP, Whiteway M. 2022. SAGA complex subunits in *Candida albicans* differentially regulate filamentation, invasiveness, and biofilm formation. Front Cell Infect Microbiol 12:764711. https://doi.org/10.3389/fcimb.2022.764711
56. Giner-Llorca M, Locascio A, Garrigues S, Manzanares P, Marcos JF. 2023. Novel findings about the mode of action of the antifungal protein PeAfpA from *Penicillium expansum*. Appl Microbiol Biotechnol 107:1491–1506. https://doi.org/10.1007/s00253-023-12749-0
57. Morschhäuser J. 2016. The development of fluconazole resistance in *Candida albicans* - an example of microevolution of a fungal pathogen. J Microbiol 54:192–201. https://doi.org/10.1007/s12275-016-5628-4
58. Prasad R, Nair R, Banerjee A. 2019. Multidrug transporters of *Candida species* in clinical azole resistance. Fungal Genet Biol 132:103252. https://doi.org/10.1016/j.fgb.2019.103252
59. Lv QZ, Yan L, Jiang YY. 2016. The synthesis, regulation, and functions of sterols in *Candida albicans*: Well-known but still lots to learn. Virulence 7:649–659. https://doi.org/10.1080/21505594.2016.1188236
60. Alimardani P, Régnacq M, Moreau-Vauzelle C, Ferreira T, Rossignol T, Blondin B, Bergès T. 2004. SUT1-promoted sterol uptake involves the ABC transporter Aus1 and the mannoprotein Dan1 whose synergistic action is sufficient for this process. Biochem J 381:195–202. https://doi.org/10.1042/BJ20040297
61. Gomez-Raja J, Davis DA. 2012. The β-arrestin-like protein Rim8 is hyperphosphorylated and complexes with Rim21 and Rim101 to promote adaptation to neutral-alkaline pH. Eukaryot Cell 11:683–693. https://doi.org/10.1128/EC.05211-11
62. Kim W, Spear ED, Ng DTW. 2005. Yos9p detects and targets misfolded glycoproteins for ER-associated degradation. Mol Cell 19:753–764. https://doi.org/10.1016/j.molcel.2005.08.010
63. Nikko E, Sullivan JA, Pelham HRB. 2008. Arrestin-like proteins mediate ubiquitination and endocytosis of the yeast metal transporter Smf1. EMBO Rep 9:1216–1221. https://doi.org/10.1038/embor.2008.199
64. Cowart LA, Obeid LM. 2007. Yeast sphingolipids: recent developments in understanding biosynthesis, regulation, and function. Biochim Biophys Acta 1771:421–431. https://doi.org/10.1016/j.bbalip.2006.08.005
65. Jiang L, Pan H. 2018. Functions of CaPhm7 in the regulation of ion homeostasis, drug tolerance, filamentation and virulence in *Candida albicans*. BMC Microbiol 18:49. https://doi.org/10.1186/s12866-018-1193-9
66. Berman J, Krysan DJ. 2020. Drug resistance and tolerance in fungi. Nat Rev Microbiol 18:319–331. https://doi.org/10.1038/s41579-019-0322-2
67. Shingu-Vazquez M, Traven A. 2011. Mitochondria and fungal pathogenesis: drug tolerance, virulence, and potential for antifungal therapy. Eukaryot Cell 10:1376–1383. https://doi.org/10.1128/EC.05184-11
68. Shen J, Ma M, Duan W, Huang Y, Shi B, Wu Q, Wei X. 2023. Autophagy alters the susceptibility of *Candida albicans* biofilms to antifungal agents. Microorganisms 11:2015. https://doi.org/10.3390/microorganisms11082015
69. Druseikis M, Mottola A, Berman J. 2023 The metabolism of susceptibility: clearing the FoG between tolerance and resistance in *Candida albicans*. Curr Clin Micro Rpt 10:36–46. https://doi.org/10.1007/s40588-023-00189-3
70. Li D, Chen H, Florentino A, Alex D, Sikorski P, Fonzi WA, Calderone R. 2011. Enzymatic dysfunction of mitochondrial complex I of the *Candida albicans* goa1 mutant is associated with increased reactive oxidants and cell death. Eukaryot Cell 10:672–682. https://doi.org/10.1128/EC.00303-10
71. Yu Q, Jia C, Dong Y, Zhang B, Xiao C, Chen Y, Wang Y, Li X, Wang L, Zhang B, Li M. 2015. *Candida albicans* autophagy, no longer a bystander: Its role in tolerance to ER stress-related antifungal drugs. Fungal Genet Biol 81:238–249. https://doi.org/10.1016/j.fgb.2015.02.008
72. Navarathna DHMLP, Das A, Morschhäuser J, Nickerson KW, Roberts DD. 2011. Dur3 is the major urea transporter in *Candida albicans* and is co-regulated with the urea amidolyase Dur1,2. Microbiology (Reading) 157:270–279. https://doi.org/10.1099/mic.0.045005-0
73. MacPherson S, Akache B, Weber S, De Deken X, Raymond M, Turcotte B. 2005. *Candida albicans* zinc cluster protein Upc2p confers resistance to antifungal drugs and is an activator of ergosterol biosynthetic genes. Antimicrob Agents Chemother 49:1745–1752. https://doi.org/10.1128/AAC.49.5.1745-1752.2005
74. Dias PJ, Sá-Correia I. 2014. Phylogenetic and syntenic analyses of the 12-spanner drug:H(+) antiporter family 1 (DHA1) in pathogenic *Candida species*: evolution of MDR1 and FLU1 genes. Genomics 104:45–57. https://doi.org/10.1016/j.ygeno.2014.05.005
75. Ikeh M, Ahmed Y, Quinn J. 2017. Phosphate acquisition and virulence in human fungal pathogens. Microorganisms 5:48. https://doi.org/10.3390/microorganisms5030048
76. Prasad T, Saini P, Gaur NA, Vishwakarma RA, Khan LA, Haq QMR, Prasad R. 2005. Functional analysis of CaIPT1, a sphingolipid biosynthetic gene involved in multidrug resistance and morphogenesis of *Candida albicans*. Antimicrob Agents Chemother 49:3442–3452. https://doi.org/10.1128/AAC.49.8.3442-3452.2005
77. Ricardo E, Costa-de-Oliveira S, Dias AS, Guerra J, Rodrigues AG, Pina-Vaz C. 2009. Ibuprofen reverts antifungal resistance on *Candida albicans* showing overexpression of CDR genes. FEMS Yeast Res 9:618–625. https://doi.org/10.1111/j.1567-1364.2009.00504.x
78. Heymann P, Gerads M, Schaller M, Dromer F, Winkelmann G, Ernst JF. 2002. The siderophore iron transporter of *Candida albicans* (Sit1p/Arn1p) mediates uptake of ferrichrome-type siderophores and is required for epithelial invasion. Infect Immun 70:5246–5255. https://doi.org/10.1128/IAI.70.9.5246-5255.2002
79. Sun N, Fonzi W, Chen H, She X, Zhang L, Zhang L, Calderone R. 2013. Azole susceptibility and transcriptome profiling in *Candida albicans*

mitochondrial electron transport chain complex i mutants. Antimicrob Agents Chemother 57:532–542. https://doi.org/10.1128/AAC.01520-12
80. Brown AJ, Budge S, Kaloriti D, Tillmann A, Jacobsen MD, Yin Z, Ene IV, Bohovych I, Sandai D, Kastora S, Potrykus J, Ballou ER, Childers DS, Shahana S, Leach MD. 2014. Stress adaptation in a pathogenic fungus. J Exp Biol 217:144–155. https://doi.org/10.1242/jeb.088930
81. Berman J, Sudbery PE. 2002. *Candida albicans*: a molecular revolution built on lessons from budding yeast. Nat Rev Genet 3:918–931. https://doi.org/10.1038/nrg948
82. Leek JT, Scharpf RB, Bravo HC, Simcha D, Langmead B, Johnson WE, Geman D, Baggerly K, Irizarry RA. 2010. Tackling the widespread and critical impact of batch effects in high-throughput data. Nat Rev Genet 11:733–739. https://doi.org/10.1038/nrg2825
83. Love MI, Huber W, Anders S. 2014. Moderated estimation of fold change and dispersion for RNA-seq data with DESeq2. Genome Biol 15. https://doi.org/10.1186/s13059-014-0550-8
84. Borman AM, Szekely A, Johnson EM. 2016. Comparative pathogenicity of United Kingdom isolates of the emerging pathogen *Candida auris* and other key pathogenic *Candida species*. mSphere 1:e00189-16. https://doi.org/10.1128/mSphere.00189-16
85. Kean R, Delaney C, Sherry L, Borman A, Johnson EM, Richardson MD, Rautemaa-Richardson R, Williams C, Ramage G. 2018. Transcriptome assembly and profiling of *Candida auris* reveals novel insights into biofilm-mediated resistance. mSphere 3:e00334-18. https://doi.org/10.1128/mSphere.00334-18
86. Chow NA, Muñoz JF, Gade L, Berkow EL, Li X, Welsh RM, Forsberg K, Lockhart SR, Adam R, Alanio A, Alastruey-Izquierdo A, Althawadi S, Araúz AB, Ben-Ami R, Bharat A, Calvo B, Desnos-Ollivier M, Escandón P, Gardam D, Gunturu R, Heath CH, Kurzai O, Martin R, Litvintseva AP, Cuomo CA. 2020. Tracing the evolutionary history and global expansion of *Candida auris* using population genomic analyses. mBio 11:e03364–19. https://doi.org/10.1128/mBio.03364-19
87. Kim JS, Cha H, Bahn YS. 2024. Comprehensive overview of *Candida auris* : an emerging multidrug-resistant fungal pathogen . J Microbiol Biotechnol 34:1365–1375. https://doi.org/10.4014/jmb.2404.04040
88. Váradi G, Bende G, Borics A, Dán K, Rákhely G, Tóth GK, Galgóczy L. 2024. Rational design of antifungal peptides based on the γ-core motif of a *Neosartorya* (*Aspergillus*) *fischeri* antifungal protein to improve structural integrity, efficacy, and spectrum . ACS Omega 9:7206–7214. https://doi.org/10.1021/acsomega.3c09377
89. Ignasiak K, Maxwell A. 2017. Galleria mellonella (greater wax moth) larvae as a model for antibiotic susceptibility testing and acute toxicity trials. BMC Res Notes 10:428. https://doi.org/10.1186/s13104-017-2757-8
90. Piatek M, Sheehan G, Kavanagh K. 2021. *Galleria mellonella*: the versatile host for drug discovery, *in vivo* toxicity testing and characterising host-pathogen interactions. Antibiotics (Basel) 10:1545. https://doi.org/10.3390/antibiotics10121545
91. Giammarino A, Bellucci N, Angiolella L. 2024. *Galleria mellonella* as a model for the study of fungal pathogens: advantages and disadvantages. Pathogens 13:233. https://doi.org/10.3390/pathogens13030233
92. Copping VMS, Barelle CJ, Hube B, Gow NAR, Brown AJP, Odds FC. 2005. Exposure of *Candida albicans* to antifungal agents affects expression of SAP2 and SAP9 secreted proteinase genes. J Antimicrob Chemother 55:645–654. https://doi.org/10.1093/jac/dki088
93. El-Houssaini HH, Elnabawy OM, Nasser HA, Elkhatib WF. 2019. Influence of subinhibitory antifungal concentrations on extracellular hydrolases and biofilm production by *Candida albicans* recovered from Egyptian patients. BMC Infect Dis 19:54. https://doi.org/10.1186/s12879-019-3685-0
94. Jenull S, Tscherner M, Kashko N, Shivarathri R, Stoiber A, Chauhan M, Petryshyn A, Chauhan N, Kuchler K. 2021. Transcriptome signatures predict phenotypic variations of *Candida auris*. Front Cell Infect Microbiol 11:662563. https://doi.org/10.3389/fcimb.2021.662563
95. Johnson CJ, Davis JM, Huttenlocher A, Kernien JF, Nett JE. 2018. Emerging fungal pathogen *Candida auris* evades neutrophil attack. mBio 9:e01403–18. https://doi.org/10.1128/mBio.01403-18
96. Holt AM, Nett JE. 2024. Innate immune response to *Candida auris*. Curr Opin Microbiol 80:102510. https://doi.org/10.1016/j.mib.2024.102510
97. Bolger AM, Lohse M, Usadel B. 2014. Trimmomatic: a flexible trimmer for Illumina sequence data. Bioinformatics 30:2114–2120. https://doi.org/10.1093/bioinformatics/btu170
98. Dobin A, Davis CA, Schlesinger F, Drenkow J, Zaleski C, Jha S, Batut P, Chaisson M, Gingeras TR. 2013. STAR: ultrafast universal RNA-seq aligner. Bioinformatics 29:15–21. https://doi.org/10.1093/bioinformatics/bts635
99. Liao Y, Smyth GK, Shi W. 2014. featureCounts: an efficient general purpose program for assigning sequence reads to genomic features. Bioinformatics 30:923–930. https://doi.org/10.1093/bioinformatics/btt656
100. Ashburner M, Ball CA, Blake JA, Botstein D, Butler H, Cherry JM, Davis AP, Dolinski K, Dwight SS, Eppig JT, Harris MA, Hill DP, Issel-Tarver L, Kasarskis A, Lewis S, Matese JC, Richardson JE, Ringwald M, Rubin GM, Sherlock G. 2000. Gene Ontology: tool for the unification of biology. Nat Genet 25:25–29. https://doi.org/10.1038/75556
101. Aleksander SA, Balhoff J, Carbon S, Cherry JM, Drabkin HJ, Ebert D, Feuermann M, Gaudet P, Harris NL, Hill DP, et al. 2023. The gene ontology knowledgebase in 2023. Genetics 224:iyad031. https://doi.org/10.1093/genetics/iyad031
102. Kanehisa M, Goto S. 2000. KEGG: kyoto encyclopedia of genes and genomes. Nucleic Acids Res 28:27–30. https://doi.org/10.1093/nar/28.1.27
103. Wickham H. 2016. Ggplot2: elegant graphics for data analysis. Springer International Publishing, Cham/New York, NY.
104. Barrett T, Wilhite SE, Ledoux P, Evangelista C, Kim IF, Tomashevsky M, Marshall KA, Phillippy KH, Sherman PM, Holko M, Yefanov A, Lee H, Zhang N, Robertson CL, Serova N, Davis S, Soboleva A. 2013. NCBI GEO: archive for functional genomics data sets--update. Nucleic Acids Res 41:D991–5. https://doi.org/10.1093/nar/gks1193